University of Stavanger

Faculty of Science and Technology

MASTER'S THESIS

Study program/ Specialization: Petroleum Engineering/Reservoir Engineering	Spring semester, 2015 Open / ~~Restricted access~~
Writer: Kaia Olsen	…… (Writer's signature)
Faculty supervisor: Merete V. Madland External supervisor(s):	
Thesis title: The Impact of Temperature and Non-Carbonate Minerals on Chalk Compaction	
Credits (ECTS): 30	
Key words: • Chalk • Water weakening • $MgCl_2$ • Hydrostatic loading • Creep • Temperature effects • Mons • Kansas	Pages: 85 + enclosure: 0 Stavanger, 15.06.2015

Front page for master thesis
Faculty of Science and Technology
Decision made by the Dean October 30th 2009

The Impact of Temperature and Non-Carbonate Minerals on Chalk Compaction

by

Kaia Olsen

Thesis submitted in fulfillment of
the requirements for the degree of
Master in Petroleum Engineering

University of Stavanger
The Faculty of Science and Technology
Department of Petroleum Engineering
2015

Abstract

There has been a considerable research activity concerning the effect of brine chemistry on the mechanical behaviour of chalk since the discovery of the Ekofisk subsidence in the North Sea. Although the research on water weakening on chalk are extensive, the mechanism behind the weakening is still not fully understood. The objective of this thesis was to investigate how chalk mechanics are affected by different temperatures and chalk types during flooding of $MgCl_2$ brine. Mechanical tests were performed on 130, 92 and 60°C for two different outcrop chalk types; Mons (Belgium) and Kansas (Niobrara, US). The cores were loaded hydrostatically above yield up to a confining pressure of 14 MPa (Mons) or 24 MPa (Kansas) with a pore pressure of 0.7 MPa, followed by a 60 days creep phase of constant stress and temperature. Fractioned effluent were analysed by an ion chromatograph and microscopic studies of the tested core by SEM-EDS were performed.

During hydrostatic loading no significant difference in yield strength and in the bulk modulus was observed for Kansas chalk when comparing the test at different temperatures. While for the Mons chalk a difference between the core tested at 130°C was seen compared to the cores tested at lower temperatures (60 and 92°C). At 130°C Mons compacts less than at lower temperatures. During creep phase, on the other hand, temperature dependency on chalk compaction was observed for both Mons and Kansas chalk. Accelerating creep was observed for the core testes at 130°C causing a significant higher creep strain compared to the cores tested at lower temperatures. From ion chromatograph analysis, the dissolution-precipitation process between magnesium and calcium was seen to more or less have a one-to-one relationship. Magnesium precipitation and calcium dissolution increased with increasing temperature, which resulted in a higher core mass loss and more compaction as magnesium has a lower molar weight than calcium. These results were confirmed by higher core mass loss for higher temperatures. SEM-EDS analysis also confirmed these results when three cores, one for each testing temperature, were studied. The wt% of magnesium in the core was seen to increase with increasing testing temperature. Precipitation of magnesite was detected by the inlet side of the Mons core tested at 130°C.

Analysis of effluent pH indicated that for cores tested at 130°C the pH is more or less the same as injected brine pH (5.5-6.0), while for cores tested at lower temperatures (60 and 92°C) the pH seemed to be higher (6.1-6.5) compared to injected brine pH.

Acknowledgements

First I would like to express my gratitude towards my supervisor Professor Merete Vadla Madland for including me in the research group at the University of Stavanger and National IOR Center of Norway and her for insightful feedback throughout the writing of this thesis.

I would like to express the deepest appreciation to Reidar Inge Korsnes (PhD) for the excellent guidance and assistance in the laboratory work as well as his enthusiastic encouragement. I am also grateful for his help to develop my understanding of this subject and the feedback during the writing of this thesis.

Thanks very much to Wenxia Wang for the helps in laboratory work and SEM analysis. My sincere thanks also go to Maiya Medetbekova for the great collaboration throughout the experimental work of this thesis.

I would also like to thank Inger Karin Dirdal for introducing me to LaTeX and for all support and help I received when I faced LaTeX related problems.

Finally I will give a special thank to my beloved Trond Stødle for being patient and supporting during the work with this thesis.

Contents

List of Figures

List of Tables

1 Introduction

1.1 Background

Chalk is an important oil and gas producing reservoir rock in the North Sea. The chalk reservoirs often appears as high porosity soft rocks, but the softness of the chalk can lead to unwanted compaction of the reservoirs when pore pressure reduces during primary production. Although reservoir compaction contributes to drive hydrocarbons towards the production facilities, it can also cause the sea floor to subside. Reservoir compaction and sea floor subsidence may induce operational problems like platform safety concerns, reduced well bore stability and increased casing failures.

Probably the best known example of subsidence is the sea floor subsidence observed at the Ekofisk field. The subsidence was discovered in 1984 by observant workers that saw that the Ekofisk tank was closer to the sea level at that time compared to when it was installed. As a solution to the problem, the Ekofisk platform was jacked up 6 meters and water injection into the reservoir was implemented in order to give pressure support and prevent further compaction. Although the reservoir was repressurized to initial condition in the waterflooded areas, the compaction did not stop. Despite the stable reservoir pressure, subsidence continued at a rate of 40-50 cm/year over the next years. Today, the subsidence have reached approximate 10 meters, and the sea floor is still subsiding, but now at a lower rate of about 10 cm/year (Mathiesen, 2005). The injected water appeared to have a weakening effect on the chalk reservoir, and this phenomenon is referred to as the water-weakening effect.

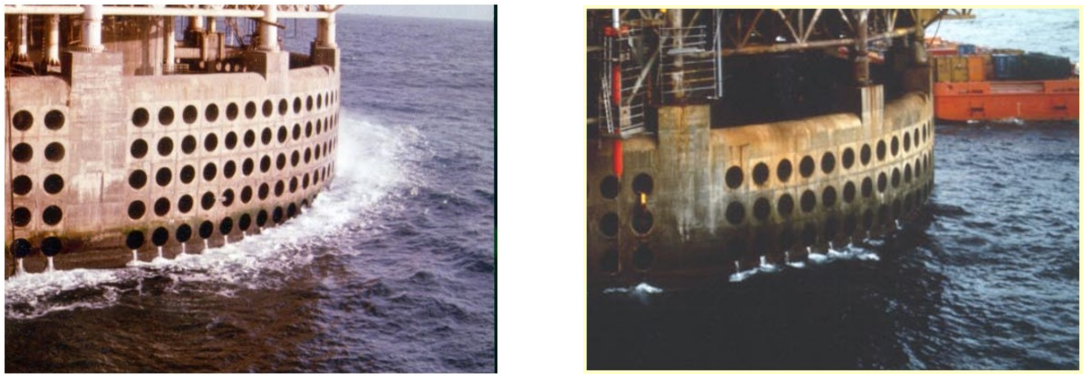

(a) 1978 (b) 1986

Figure 1.1: *Pictures of the Ekofisk tank, showing difference in relative sea level from 1978 to 1986. (Zornes, 2004)*

Since the Ekofisk subsidence was observed in 1984, there has been a considerable research activity concerning the effect of brine chemistry. Several different mechanisms have been suggested to

explain the water-weakening effect of chalk, but the water-weakening effect is still not completely understood. Newman (1985) discussed water weakening of chalk as a consequence of calcium carbonate dissolution, but his theory have received limited attention due to the low solubility of calcium carbonate in water. Capillary forces was suggested by Delage et al. (1996), that argued that residual water menisci in the chalk pores are contributing to cohesion by pulling the grains together. As water is injected into the chalk, the water menisci disappear and the chalk becomes weaker. However, Risnes and Flaageng (1999) experienced that methanol-saturated chalk was stronger than water-saturated chalk, and as methanol is miscible with water, capillary forces is absent. Hence, capillary forces alone cannot fully explain the water weakening effects. Pressure solution as a water weakening mechanism has been discussed by Hellmann et al. (2002). Hellmann et al. (2002) argued that when chalk grains are exposed to stress, the chemical instabilities are higher at the grain-to-grain contacts causing dissolution at the contacts. Further Hellmann et al. (2002) explain that dissolved material from the grain-to-grain contacts are transported by fluid flow to regions with lower stress and precipitate, resulting in compaction of the chalk. (see Fig. 1.2 for illustration). Risnes et al. (2003, 2005) agreed with the suggested pressure solution by Hellmann et al. (2002), but argued that adsorption pressures between chalk grains caused by attraction of water molecules onto the chalk surface also was an important mechanism. Heggheim et al. (2004) performed mechanical tests on chalk cores saturated with brines with different salinities, and did not observe any correlation between the attraction of water molecules to the chalk surface and the weakening of chalk, as suggested by Risnes et al. (2003). Heggheim et al. (2004) believed that the difference in mechanical strength of the cores observed in their tests most reasonably was explained by chemical effects, and concluded that the observed water weakening was a result of chemical dissolution-precipitation

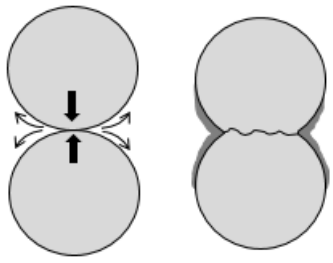

Figure 1.2: *Illustration of pressure solution where rock grains are subjected stress. Dissolution and diffusion occurs at the grain-to-grain boundary and precipitation occurs in pore spaces. The net result is compaction of the grains.*

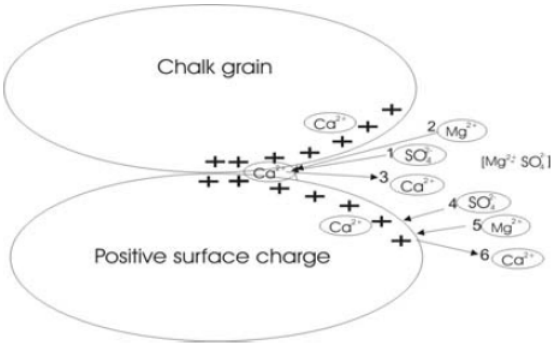

Figure 1.3: *Illustration of the Ca/Mg substitution mechanism where magnesium (Mg^{2+}) ions substitutes calcium (Ca^{2+}) ions on the chalk surface in the presence of sulphate (SO_4^{2-}) (Korsnes et al., 2006a).*

processes at chalk surface.

Ion substitution as a water-weakening mechanism has been discussed by Korsnes et al. (2006a). Korsnes et al. (2006a) studied the mechanical behaviour of chalk when flooding cores with distilled water, seawater without sulphate and seawater with sulphate at 130°C. Korsnes et al. (2006a) observed an increase in compaction for cores flooded with seawater that contained sulphate, while for cores flooded without sulphate present in the seawater, the compaction of the core was comparable to distilled water. Korsnes et al. (2006a) concluded that when sulphate is present in the fluid, magnesium ions from the brine substitutes calcium ions at the chalk surface resulting in weakening of chalk as magnesium ions are smaller than calcium ions (Fig. 1.3). However, Madland et al. (2011) performed flooding experiments at 130°C with pure magnesium chloride ($MgCl_2$) brine without sulphate and observed weakening of the chalk. Hence, sulphate is not needed in order to have a significant amount of chemical deformation.

Although it is proved that sulphate is not needed to observe water weakening of chalk, the presence of sulphate in the flooding fluid has been shown to have a significant effect on chalks mechanical strength at high temperatures (Korsnes et al., 2007; Megawati et al., 2012). Megawati et al. (2012) demonstrated that the mechanical yield and bulk modulus of chalk are reduced by increasing sulphate concentration at high temperature (130°C), and that the same effects are more or less absent at lower temperatures (50°C). Megawati et al. (2012)discussed the sulphate effects in terms of surface charge, and suggested that sulphate adsorb to the chalk surface causing the negatively charged surface to be neutralized by a diffusive layer closet to the surface. Megawati et al. (2012) explained that close to grain-to-grain contacts the diffusive layer from each grain surface will overlap and give rise to a repulsive force, which can be described by the disjoining pressure if two charged surfaces approach each other (Fig. 1.4).

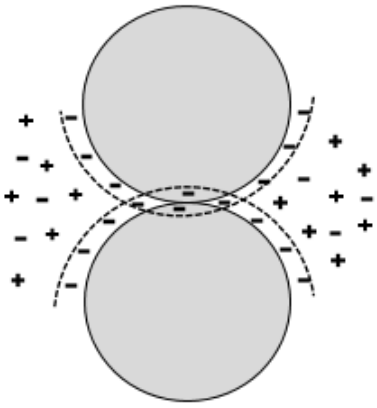

Figure 1.4: *Illustration of negatively charged chalk surface with weak overlap of electrical double layer (denoted by dashed line) and electrostatic repulsive forces between the two surfaces.*

In the resent years the dissolution-precipitation process between magnesium and calcium has received much attention (Madland et al., 2011; Nermoen et al., 2015; Zimmermann et al., 2015), and

this is the mechanicm that will be studied in this thesis. As brines containing magnesium (eg. $MgCl_2$) is injected into chalk, magnesium bearing minerals (eg. magnesite) have been observed to precipitate inside the core, while calcium has been observed to dissolved from the chalk in that process As magnesium ions are smaller in size than calcium ions, the result of the dissolution-precipitation process is compaction of the chalk.

1.2 Purpose of this study

As described in the previous section, there are several mechanisms that are suggested to explain the water-weakening effect of chalk. The chalk mechanics seems to be affected by many factors, and the objective of this thesis is to investigate how the mechanics are affected by different temperatures and chalk types during flooding of magnesium chloride ($MgCl_2$) brine. This was done by performing almost identical experiments where only temperature and chalk type were a changing factor. By doing this, all other factors would have equal effect on the water weakening of the chalk cores, which means that any difference in the results between the experiments would be an effect of temperature and/or chalk difference.

Experimental testing temperatures of interest were 60, 92 and 130°C, as reservoir temperature of the North Sea chalk fields Valhall and Ekofisk are 92 and 130°C, respectively. While 60°C were used because no significant effects of temperature differences is expected to be observed below 70°C. Two different types of chalk (Mons from Harmignies, Belgium and Kansas from Niobrara, US) were used for experiments at each temperature in order to avoid the risk of generalizing on specific properties of one chalk type.

The experiments were performed in co-operation with another master student, Maiya Medetbekova.

2 Theory

2.1 Chalk

Chalk is a sedimentary carbonate rock that mainly contain calcite which is a crystal form of calcium carbonate ($CaCO_3$). Chalk is built up of whole and fragmentary parts of calcite skeletons produced by planktonic algae, known as coccolithophorids. The building blocks of the skeletons of coccolithophorids are calcite tables or plateles with a size of 0.5 to 1 μm which are arranged in rings and rosettes known as coccoliths. The dimension of coccoliths are in the order of $3 - 15\mu$m in diameter (Fig. 2.1). The coccoliths are in turn arranged into a hollow coccosphere that encoses the soft part of the organism (Kennedy, 1985). Upon death, the soft part decay and the coccospheres becomes a part of the surrounding sediments. The coccospheres are in turn decayed into platelets and coccoliths. Complete coccospheres are rarely found in chalk.

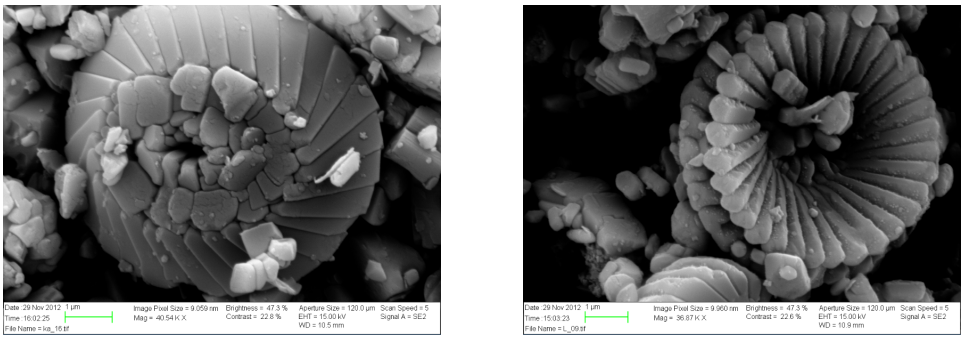

(a) (b)

Figure 2.1: *SEM Images of intact coccoliths found in a Kansas outcrop chalk from the Niobrara quarry in US (a) and Liége outcrop chalk from near Liége in Belgium (b) (Images by Wenxia Wang, University of Stavanger).*

Chalk outcrops used the experiments for this thesis consist of a mixture of intact and fragmented coccolith rings of different size, which give the chalk an open structure where the dimensions of the pore space may be considerably greater than the dimensions of the individual grains. This gives the chalk a high porosity, but a rather small permeability due to narrow pore throats. Typical permeability values are in the range of 1 to 5 md (Risnes et al., 2003). Nevertheless, chalk reservoirs can have high permeabilities in range of 100 md due to fractured systems inside the formation. North Sea chalk reservoirs appears as high porosity soft rocks, due to absence of normal diagenetic processes. This makes the properties of North Sea chalk reservoir similar to outcrop chalk, which makes it possible to perform systematic studies on chalk properties on outcrop chalk (Risnes et al., 2005).

2.2 Mechanical Properties of Rocks

General theory about rock mechanics is based on the books "Petroleum Related Rock Mechanics" by Fjær et al. (2008) and "Petroleum Reservoir Rock and Fluid Properties" by Dandekar (2006).

2.2.1 Stress

Stress refers to the force applied to a rock that tends to change its dimensions. The external force applied to a rock is normally referred to as load. Stress (σ) is defined as,

$$\sigma = \frac{F}{A} \tag{2.1}$$

where F is a force acting through a cross-section A. The SI unit for stress is Pascal (Pa). In rock mechanics positive stress refers to *compressive* stresses, i.e compaction of a material, while negative stress refers to *tensile* stresses, i.e stretching of a material. When studying deformation of a porous material containing fluids in a closed pressurized system, the grains only experience the effective stress and not the total stress applied to the material. The effective stress is the difference between the total stress and the pore fluid pressure as illustrated in Fig. 2.2. The effective stress (σ') is defined as,

$$\sigma' = \sigma_{tot} - \alpha P_f \tag{2.2}$$

where σ' is effective stress, σ_{tot} is total stress, α is Biot coefficient and P_f is pore pressure. The Biot coefficient, also called the effective stress coefficient, is interpreted as the fluid-to-solid contact area by the total representative area when projected to an arbitrary plane (Nermoen et al., 2013). The fluid-to-solid contact area is illustrated in Fig. 2.3. Nermoen et al. (2013) estimated the Biot coefficient to be in the order of 0.85 to 1 for chalks. As the pore pressure was relatively low ($P_f = 0.7MPa$) in the experiments performed in this thesis, the Biot coefficient was not important and it was put to 1. In this study, the radial stress (σ_{rad}) was calculated from the effective stress equation (Eq. (2.2)) as followed,

$$\sigma_{rad} = \sigma_{tot} - P_f \tag{2.3}$$

In the calculation of axial stress (σ_{ax}), the friction pressure necessary to keep the piston down at the core had to be accounted for. Hence, axial strain was calculated according to,

$$\sigma_{ax} = \sigma_{rad} + f_{area}(P_{pist} - P_{fric}) \tag{2.4}$$

where f_{area} is an area factor for the piston pressure chamber and the cross area of the plug, P_{pist} is piston pressure, and P_{fric} is the frictional pressure of the piston movement in the triaxial cell. For the experiments performed in this study f_{area} was 1.265 and P_{fric} was ~0.4 MPa. As P_{pist} was kept at approximately 0.7 MPa during the experiments, the relation $P_{pist} - P_{fric}$ was set to ~0.3 in the calculations.

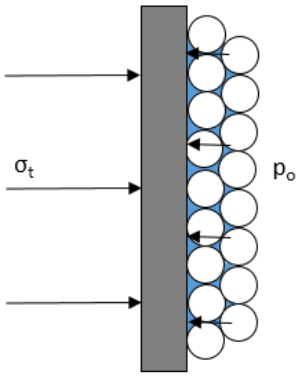

Figure 2.2: *Illustration of a porous material under stress where the grains only experiences the effective stress (Davidsen, 2011).*

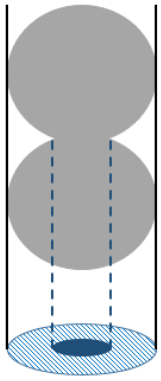

Figure 2.3: *Microscopic view of the fluid-solid contact area (in gradient blue) in which the fluid-solid force exchange may occur (Nermoen et al., 2013).*

2.2.2 Strain

Strain is a dimensionless measurement of the relative change in shape or size of a rock due to applied stress. In other words, strain is a measure of the deformation of a material when a load is applied (Dandekar, 2006). Rock mechanical experiments are usually performed on cylindrical cores that will deform in both axial and radial directions. The experiments performed in this study were not equipped with radial compaction measurement. Thus, only axial compaction was measured. Axial strain (ε_{ax}) is defined as a ratio of change in length to original length,

$$\varepsilon_{ax} = \frac{L - L_0}{L_0} \tag{2.5}$$

where L_0 is the initial length prior to deformation and L is the new core length after deformation. Often it is also convenient to express the deformation with respect to relative change in volume. Volumetric strain (ε_{vol}) is defined in a similar way,

$$\varepsilon_{vol} = \frac{V - V_0}{V_0} \tag{2.6}$$

where V is the initial bulk volume of the core prior to deformation and V_0 is the bulk volume after deformation. In mechanical experiments, the volumetric strain is commonly calculated according to,

$$\varepsilon_{vol} = \varepsilon_{ax} + 2\varepsilon_{rad} + 2\varepsilon_{ax}\varepsilon_{rad} + \varepsilon_{rad}^2 + \varepsilon_{ax}\varepsilon_{rad}^2 \tag{2.7}$$

But as the experiments performed for this thesis were not equipped with radial measurement, only axial strain was known. By assuming isotropic condition, the volumetric strain was estimated according to,

$$\varepsilon_{vol} = 3\varepsilon_{ax} \tag{2.8}$$

As chalk is not an isotropic material, this estimation of volumetric strain is not exact. Experimental research by Korsnes et al. (2006b) showed that chalk is anisotropic. All mechanical properties, except permeability and tensile strength, showed anisotropic behaviour.

2.2.3 Stress-Strain Relations

In most material as stress increases, strain also increases. Two types of stress-strain relation is commonly observed for chalk; *elastic* and *plastic* deformation. In a stress vs. strain plot, elastic deformation is observed to have a linear trend (Fig. 2.4). By increasing stress and strain with time, the rock will reach its yield point and become a subject of plastic deformation, where strain will increase more with less applied force (stress) than seen in the elastic region.

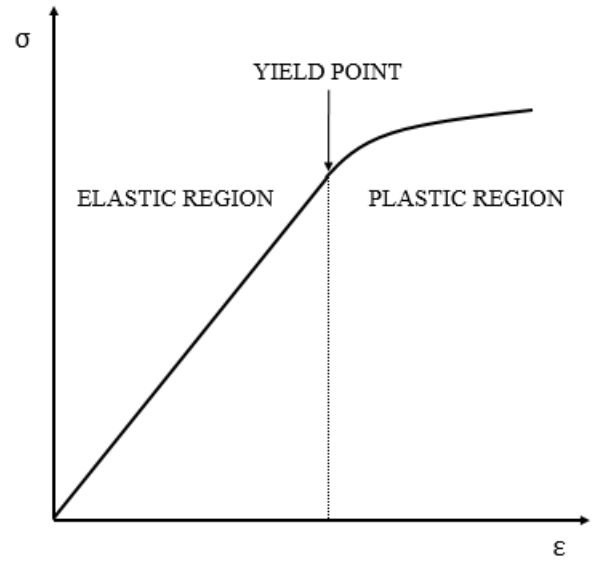

Figure 2.4: *Stress vs. strain for a deforming material illustrating yield point and elastic and plastic region.*

Bulk modulus is an elastic parameter that measure the materials resistance against hydrostatic

loading. Bulk modulus (K) is defined as the ratio of hydrostatic stress (σ_p) relative to the volumetric strain (ε_{vol}),

$$K = \frac{\sigma_p}{\varepsilon_{vol}} \tag{2.9}$$

During hydrostatic loading, when a material is in a hydrostatic stress state it means that the material experience the same stress from all directions, $\sigma_p = \sigma_x = \sigma_y = \sigma_z$, while shear stresses equals zero, $\tau_{xy} = \tau_{yz} = \tau_{xz} = 0$. In this study, hydrostatic tests were performed because of its good repeatability. Hydrostatic tests can be performed under drained or undrained conditions. The tests performed in this study were undrained hydrostatic testes. In such tests, the slope of the stress versus volumetric strain curve gives the bulk modulus of the rock.

2.2.4 Creep

Creep is a time-dependent deformation that may occur in materials under constant stress and temperature. In hydrostatic tests on chalk it is commonly observed that the deformation rate decreases with time in the beginning, and stabilizes and becomes constant after some time. For some chalk types, under certain conditions, it can be observed that the deformation rate accelerates after some time with constant rate. An illustration of a material with accelerating creep strain is presented in Fig. 2.5.

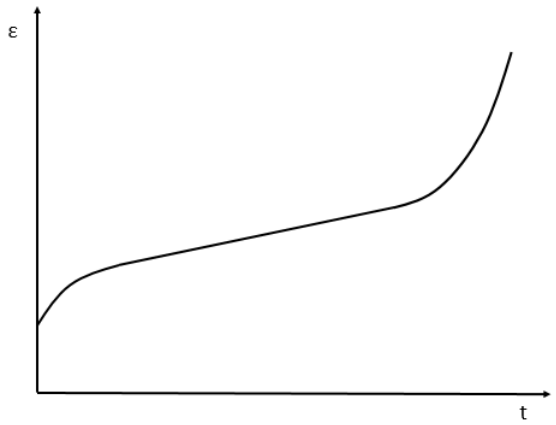

Figure 2.5: *Strain versus time for a creeping material, where deformation rate accelerate after some time of constant rate.*

2.2.5 Calculation of Porosity, Pore volume, Bulk Volume, and Density

Porosity is a rock property that measure the potential storage volume in a rock. Porosity (ϕ) is defined as,

$$\phi = \frac{V_p}{V_b} \tag{2.10}$$

where V_p is the pore volume of the rock and V_b the total bulk volume. In this study, three different methods were used to calculate porosity. The first method uses bulk volume and mass difference between dry and saturated core,

$$\phi_1 = \frac{V_p}{V_b} = \frac{m_{sat} - m_{dry}}{\rho_{water} V_b} \tag{2.11}$$

where m_{sat} and m_{dry} is the weight of water saturated and dry core, respectively, and ρ_{water} the density of the water. Index number 1 refer to method 1. The second method calculates the porosity after testing by considering change in volumetric strain,

$$\phi_2 = \frac{V_p + \Delta V_b}{V_b + \Delta V_b} = \frac{\phi_0 + \varepsilon_{vol}}{1 + \varepsilon_{vol}} \tag{2.12}$$

where ϕ_0 is original porosity and ε_{vol} is volumetric strain which were calculated according to Eq. (2.8). The third method takes into account the change in solid density,

$$\phi_3 = 1 - \frac{V_s}{V_b} = 1 - \frac{m_{sat}}{\rho_s V_b} \tag{2.13}$$

where V_s is the solid volume of the core and ρ_s the solid density. When calculating porosity after testing, method 1 and 3 (Eq. (2.11) and (2.13), respectively) accounts for chemical changes in the core by including mass and density changes, while method 2 (Eq. (2.11)) look at porosity from a pure mechanical point of view by estimating porosity only from volumetric changes. Method 3 gives the same result as method 1 when the solid density is calculated as the fraction of dry weight (m_{dry}) over the volume of solids (V_s),

$$\rho_s = \frac{m_{dry}}{V_s} = \frac{m_{dry}}{V_b - V_p} \tag{2.14}$$

Hence, an additional density estimation were used for calculation of porosity from Eq. (2.13). After testing, average density was determined by cutting the cores into smaller pieces and using a gas pycnometer to measure the volume of the chalk pieces. Density of each measured piece (ρ_i) in addition to the average density of the cores ($\overline{\rho}$) are calculated from the following formulas,

$$\rho_i = \frac{m_i}{V_i} \tag{2.15}$$

$$\overline{\rho} = \sum_i \left(\frac{m_i}{\sum_i m_i} \right) \rho_i \tag{2.16}$$

where m_i is mass weight and V_i measured volume of the chalk pieces. The gas pycnometer used a gas displacement method to measure the solid volume of the core pieces inside the pycnometer pot. The gas used in this study was helium.

The bulk volume (V_b) is given by the sum of the volume of the solids (V_s) and the pores (V_p),

$$V_b = V_s + V_p \tag{2.17}$$

Before testing, the cores had a cylindrical shape and the initial bulk volume was simply given by the volume of a cylinder,

$$V_b = \frac{1}{4}\pi L D^2 \tag{2.18}$$

where L is the length and D the diameter of the core. After testing the cores were non-homogeneously deformed and the bulk volume was then found by measuring the average diameter at intervals along the cores, calculate the volume between each interval and sum these volumes to get the bulk volume. Average diameter at each interval was found by measuring the diameter at three points around the axis of the core and calculate an average value. The volume between each interval was given by,

$$V_i = \frac{\pi(L_{i+1} - L_i)}{3}(r_{i+1}^2 + r_{i+1}r_i + r_i^2) \tag{2.19}$$

where $L_{i+1} - L_i$ is the length of the interval and r_{i+1} and r_i is the radius in the beginning and end of the interval respectively. The bulk volume could then be determined by the sum of the volumes between the intervals,

$$V_b = \sum_i V_i \tag{2.20}$$

Bulk volume measurements before and after testing were used to estimate the total volumetric strain defined according to Eq. (2.6).

2.2.6 Estimating Changes in Solid Mass

During a flooding experiment like those performed in this thesis, minerals dissolve and precipitate causing the core mass to change over time. In this thesis, the mass change was believed to be cased by an ion substitution between magnesium and calcium inside the core. Two method was used to estimate mass loss. The first method was to measure the weight difference between dry core before and after testing. In the second method the results from ion chromatograph analysis was used to calculate the mass loss. The calculation process will be described in this section.

During the experiment the mole change (Δn_j) was calculated as the sum of the difference in concentration between each effluent sample ($\sum_i((c_{in,j} - c_{out,j})_i$) times the flooding rate (q) in l/day,

$$\Delta n_j = \sum_i (c_{in,j} - c_{out,j})_i q \tag{2.21}$$

where j is the species (magnesium and calcium) in g/mol and i indicates the time between one effluent sample and the next. If calcium precipitation was calculated to be higher than the magnesium dissolution, it was assumed that the additional calcium came from precipitation of calcium carbonate ($CaCO_3$). The mole change in carbonate was therefore simply given by,

$$\Delta n_{CO_3} = \Delta n_{CaCO_3} = \Delta n_{Ca} + \Delta n_{Mg} \tag{2.22}$$

where Δn_{Mg} had a negative value. Mass change (ΔM_s) could then be calculated as,

$$\Delta M_s = \sum_j \Delta n_j M_{w,j} \tag{2.23}$$

where $M_{w,j}$ is the molar weight of the species j in g/mol. The molecular weight of the species was 40.08, 24.31 and 60.01 mol/l for magnesium, calcium and calcium carbonate, respectively.

2.2.7 Estimating Permeability

Permeability is a rock property that measures the ability for a porous material to transmit fluids. In this thesis the permeability of the cores during testing was calculated by rewriting Darcy's law from,

$$q = -A\frac{k}{\mu}\frac{\Delta P}{\Delta L} \tag{2.24}$$

to

$$k = -\frac{q\mu\Delta L}{A\Delta P} \tag{2.25}$$

where q is the flow rate of the fluid through the core, L is the length of the core, μ is the fluid viscosity, A is the cross section area of the core, and ΔP is differential pressure from inlet to outlet of the core. The SI unit of permeability is m^2, but the most common unit is Darcy, D. Viscosity were found by using the online calculator *CREWES Fluid Property Calculator* that was designed to produce information on pore fluid of interests in petroleum exploration (CREWES, 2015).

2.3 Scanning Electron Microscopy with X-ray Microanalysis

Scanning electron microscopy with X-ray microanalysis (SEM-EDS) is a technology for analysing the chemistry characteristics of a material sample. In this thesis, SEM-EDS were used to verify the precipitation of new minerals in the chalk matrix after flooding with $MgCl_2$ brine. The technology behind SEM-EDS is that a high-energy beam of electrons is scanned across the materials surface. When an incident electron beam hits atoms of the sample, the incident beam may excite an electron in a electron shell of the atoms resulting in this electron being emitted from the shell while creating a hole where the electron used to be. If these "holes" are in inner shells, the atoms are not in stable states. In order for the atom to stabilize, an electron from an outer, higher-energy shell will drop into the inner shell filling the hole. Because the outer shell had higher energy, the energy difference between the outer and inner shell must be released, and it is released in form of a X-ray (*How SEM-EDS Works*, n.d.).

The X-rays emitted from the sample atoms are characteristics in energy and wave length, and the energy is not only characteristics for the individual atoms, but it is possible to characterize between which shells that lost electrons and which shells that replaced them. For instance, if the innermost electron shell, the K shell, of an atom is replaced by an L shell electron, a K alpha X-ray is emitted from the sample. Or if the K shell electron is replaced by a M shell electron, a K beta X-ray is emitted. The last possibility is that a L shell electron is replaced by a M shell electron, emitting a

L alpha X-ray (*How SEM-EDS Works*, n.d.). See Fig.2.6 for illustration of the different X-rays. In this thesis, only K alpha X-rays were studied for the chalk samples.

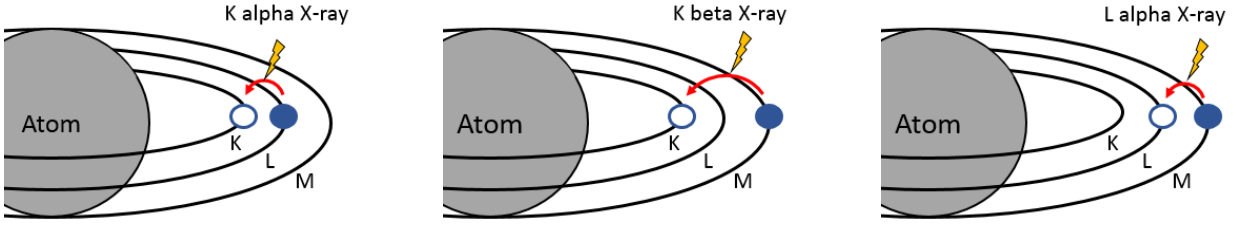

(a) *L shell electron replaces K shell electron, creating a K alpha X-ray.*

(b) *M shell electron replaces K shell electron, creating a K beta X-ray.*

(c) *M shell electron replaces L shell electron, creating a L alpha X-ray.*

Figure 2.6: *Electrons from a outer, higher-energy shell drops into "holes" in inner electron shells. Energy difference is released as X-rays (*How SEM-EDS Works*, n.d.).*

The number and energy of of the X-rays emitted from the sample atoms is measured by an energy-dispersive spectrometer (EDS). The EDS software plots the X-ray energy against the number of X-rays, resulting in a plot showing peaks for the different atoms that are found. The software calculates the area under the peaks that are selected by the operator, and from that the weight and atom percent are calculated.

3 Methodology

3.1 Core Material

Two different outcrop chalk types were used in the experimental study; Mons from the Harmignies quarry in Belgium and Kansas from the Niobrara quarry in US. The reason for using two chalk types was to avoid the risk of generalizing on specific properties of one chalk type. Although there is a great similarity between high porosity chalks, there are also differences due to depositional environments, diagenetic processes and tectonic environments (Risnes et al., 2003). Mons is a very pure chalk with more than 99% calcite content, while Kansas is regarded a rather impure chalk with a calcite content of about 97% (Megawati et al., 2015). The main characteristics of these outcrop chalks are listed in Table 3.1.

Table 3.1: *Characteristics of the chalk types used in this thesis (Megawati et al., 2015).*

Chalk type	Quarry	ϕ [%]	k [mD]	Carbonate content [%]
Mons	Harmignies, Belgium	42-44	3-5	99.70
Kansas	Niobrara, US	37-40	1-2	97.20

A total of seven experiments were performed in this study; four on Mons chalk cores and three on Kansas chalk cores. Mons cores are labeled M followed by a number, and similar Kansas cores are labeled K followed by a number. Table 3.2 gives an overview of the name of the cores and at which temperature they were tested on. The reason for using two Mons cores at 92°C (M2 and M3), was that M2 failed before the test was finished, causing the start-up of a new identical experiment on M3. The failure of M2 is described in Section 3.9.

Table 3.2: *Overview of which cores that were tested at the different temperatures.*

	130°C	92°C	60°C
Mons	M6	M2 & M3	M4
Kansas	K2	K1	K3

The cores were drilled and shaped with a lathe to the desired diameter of 38.1 mm and subsequently cut into a length of about 70 mm. Due to anisotropy on mechanical properties of chalk, all cores within each chalk type (Mons or Kansas) were taken from the same chalk block and drilled out in the same direction. By doing that all experiments were performed on chalk cores with as similar mechanical properties as possible. After shaping, the cores were dried in a drying furnace at 100°C for approximately 24 hours. Dry weight was measured before they were saturated with distilled

water. The saturation process was performed by placing the cores in a vacuum vessel and use a pump to obtain vacuum. The pump was started, and when the pressure had stabilized at a pressure of about 4×10^{-4} bar the pump was switch off and the flooding valve was opened to allow distilled water to enter the vacuum vessel. After flooding, the system was kept closed for some time before taking the cores out to ensure that the cores were saturated properly. Porosity was determined by comparing dry and saturated weight. Core data for cores used in the experiments are listed in Table 3.3.

Table 3.3: *Core data for cores used in the experiments, where Mons and Kansas cores are labeled M and K, respectively, followed by a number.*

Core	Length [mm]	Diameter [mm]	Dry weight[g]	Saturated weight[g]	Bulk volume [cm^3]	Pore volume [cm^3]	Porosity [%]
M2	73.04	38.10	129.71	164.90	83.23	35.19	42.3
M3	72.20	38.10	127.23	162.21	82.27	24,98	42.5
M4	72.47	38.10	128.13	163.20	82.58	35.07	42.5
M6	72.02	38.10	127.54	162.19	82.07	34.65	42.2
K1	71.12	38.10	139.06	168.61	81.04	29.55	36.5
K2	72.11	38.10	140.59	170.58	82.17	29.99	36.5
K3	71.32	38.10	139.49	169.04	81.27	29.55	36.4

Only three experiment could run simultaneously. Hence, in order to finish the experimental work before the thesis submission deadline, it was decided that each experiment should run until 60 days of creep time before they were stopped. The cores M6, M4 and K1 were the first to be tested. After they were stopped and the results analysed, it was observed that it would have been interesting to see how the cores would have been effected by a longer creep time. The importance of running experiments over a long time is demonstrated in recently published work by Nermoen et al. (2015). Therefore, as the next experiments were started, it was decided not to stop them after 60 days of creep, but let them run for longer time. The consequence of not stopping the last experiments, was that the results from analyses after testing on the cores (M2, M3, K2 and K3) would not be available for this thesis.

3.2 Flooding Fluid

One brine type was used for all experiments; 0.219M magnesium chloride ($MgCl_2$). The brine has an ionic strength similar to seawater (Madland et al., 2011). The ion composition of the brine is summarized in Table 3.4. The brine was prepared by dissolving 44.50 g $MgCl_2 \times 6H_2O$ salt in 1 liter

distilled water. The brine was stirred with a magnetic stirrer for one hour before filtered through 0.22 μm filter to remove any particles. The pH of the finished brine was measured.

Table 3.4: *Ion and salt composition of the* $MgCl_2$ *brine injected during mechanical tests.*

Ions	$MgCl_2$ (mol/l)
HCO_3	0.000
Cl^-	0.438
SO_4^{2-}	0.000
Mg^{2+}	0.219
Ca^{2+}	0.000
Na^+	0.000
K^+	0.000
Ion strength	0.657

3.3 Mechanical Test Equipment

3.3.1 Triaxial Cell

All experiments were performed in triaxial cells, which allows testing at high confining pressure and high temperature, i.e. reservoir condition. The main parts of the triaxial cell were the piston assembly and the confining chamber held together by a loading frame (Fig. 3.1). The piston assembly consisted of a lower and upper piston chamber with a piston in between. Fig. 3.2 presents a schematic of a triaxial cell. The piston was moved up or down by pumping oil in lower or upper piston chamber respectively. A linear voltage displacement transducer (LVDT) was placed on top of the piston in order to register axial movement of the core during testing. The core was placed between two small drainage plates within an internal flooding system. A plastic shrinking sleeve was tightly clothed around the core in order to prevent the confining oil to intrude into the core. The confining chamber was filled with oil that surrounded the core assembly. Pictures of the core assembly can be seen in Section 3.4.1. The cell was mounted together by a loading frame, that contained six steel bolts that ensured that the cell could withstand the high pressure inside the confining chamber. The cell was equipped with heating elements and a regulating system (*Omron E5CN*/*Omron E5CK*) with precise temperature control (± 0.1°C). During testing the temperature was monitored by a *Pt-100RDT* resistance temperature detector inside the cell.

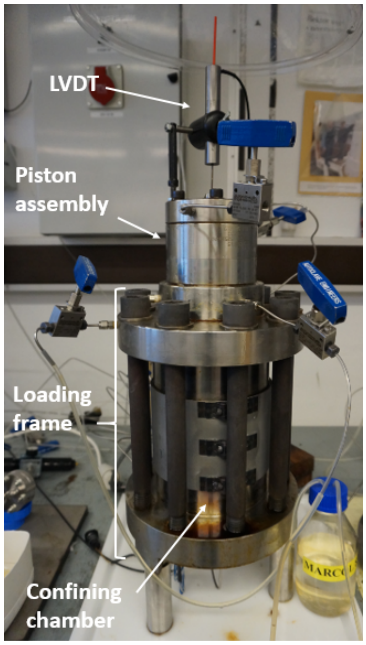

Figure 3.1: *Picture of a triaxial cell showing main parts.*

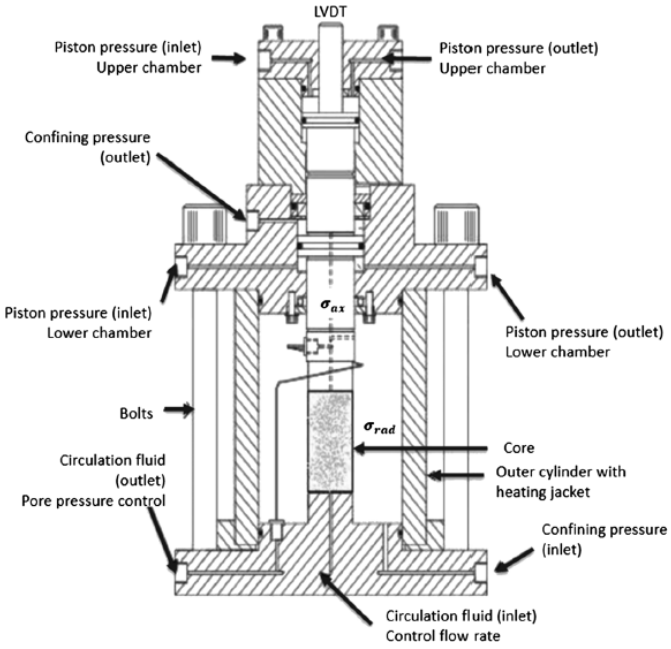

Figure 3.2: *Schematic illustrating the set-up of a triaxial cell. (Nermoen et al., 2015)*

3.3.2 Pumps and Other Auxiliary Equipment

For the experiments performed in this study, the triaxial cells were operated by three *Gilson 307 Piston Pumps* for regulating radial confining stress, piston pressure and injection flow rate. Fig. 3.3 shows a schematic of the experimental set-up which illustrate how the pumps were connected to the triaxial cell. Pump 1 pumped oil into the piston assembly to regulate the piston pressure, corresponding to the overburden pressure for a real life reservoir. Pump 2 pumped oil into the confining chamber to regulate the radial confining pressure around the core. Pump 3 regulated the flooding rate of brine into the core, and thus also the pore pressure. To avoid salt precipitation and corrosion inside the pump head/tubing, Pump 3 was connected to a flooding cell that provided the core inside the triaxial cell with brine. The flooding cell consisted of two chambers separated by a piston (Fig. 3.4). As Pump 3 pumped distilled water into the upper chamber, the piston was pushed down and brine were displaced out from the lower chamber and into the core.

Emerson Rosemount gauges were used to monitor differential pressure over the core, pore pressure, piston pressure and temperature. A back pressure regulator (BPR) was connected to the outgoing flooding line from the triaxial cell. The BPR was pressurized by CO_2 gas where the gas pressure was controlled by a valve. By using a BPR, effluent water could be sampled throughout the test period.

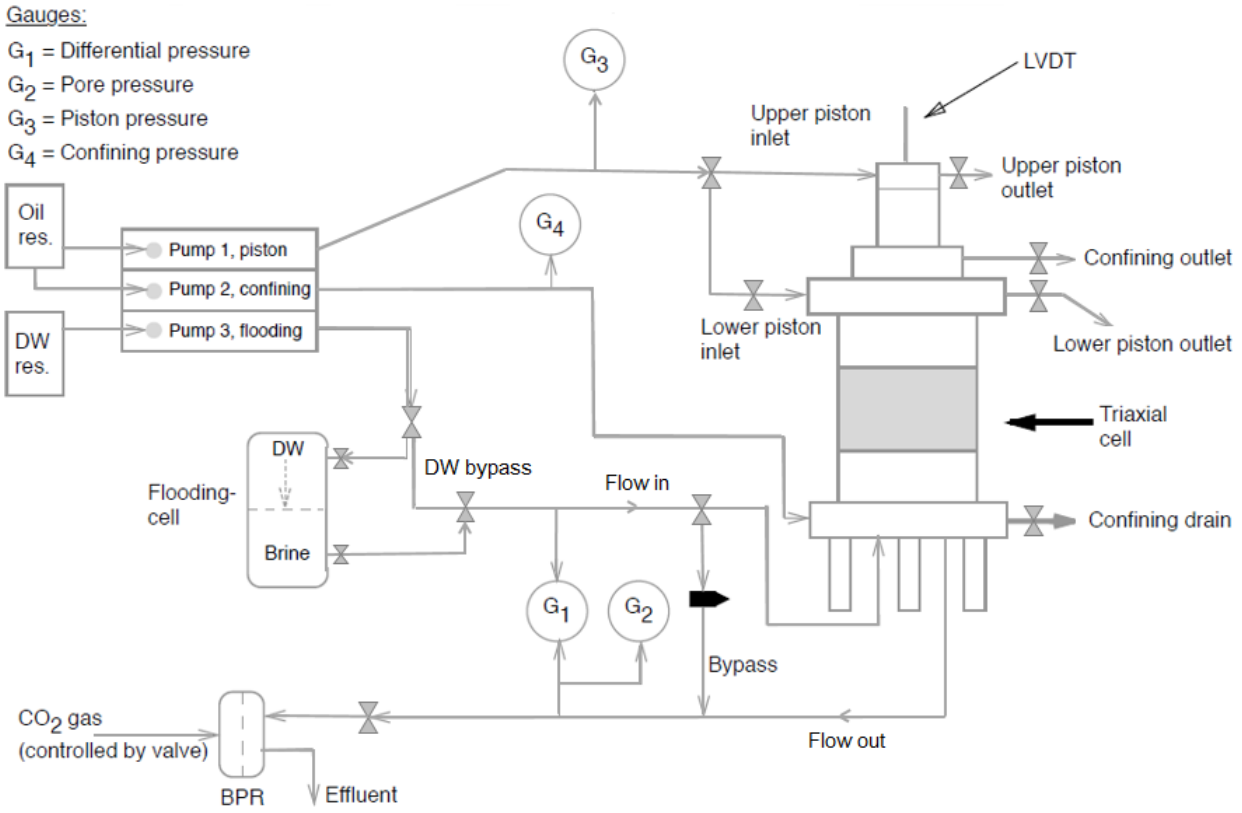

Figure 3.3: *Schematic of the experimental set-up. (Modified figure by Kjørslevik and Østensen (2014))*

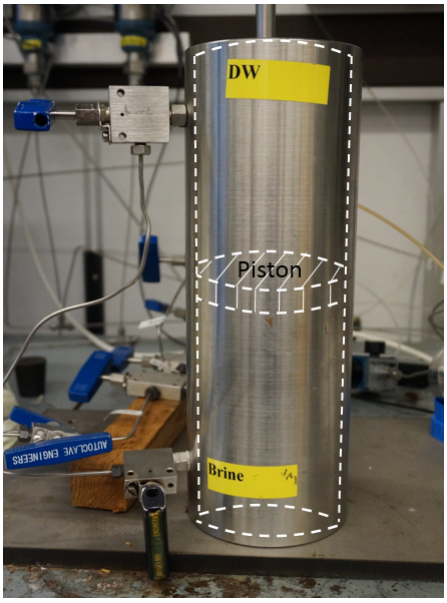

Figure 3.4: *Picture of a flooding cell where the chambers and the piston on the inside is illustrated by dashed lines. Distilled water (DW) is flooded through the upper valve into the DW chamber, which pushes the piston down resulting in brine to escape out of the lower valve from brine chamber. Brine flooding rate out of the cell equals the DW flooding rate into the cell.*

3.3.3 Software

The experimental tests were monitored and controlled by the LabView software. LabView had two main functions; controlling pump settings like pumping rate and maximum pressure, and logging data like time, axial movement, pressure and temperature values from the gauges. LabView was designed to display plots of optional variables which makes it easier to monitor the operating parameters and the experimental results during testing (see an example of a plot in Fig. 3.5 where axial movement is plotted against time during the creep phase of Mons core M3 tested at 92°C). All logged data were written to and saved in a data file that could be opened in *Microsoft Excel*. The logging interval, that decided the amount of data saved, were manually set in LabView.

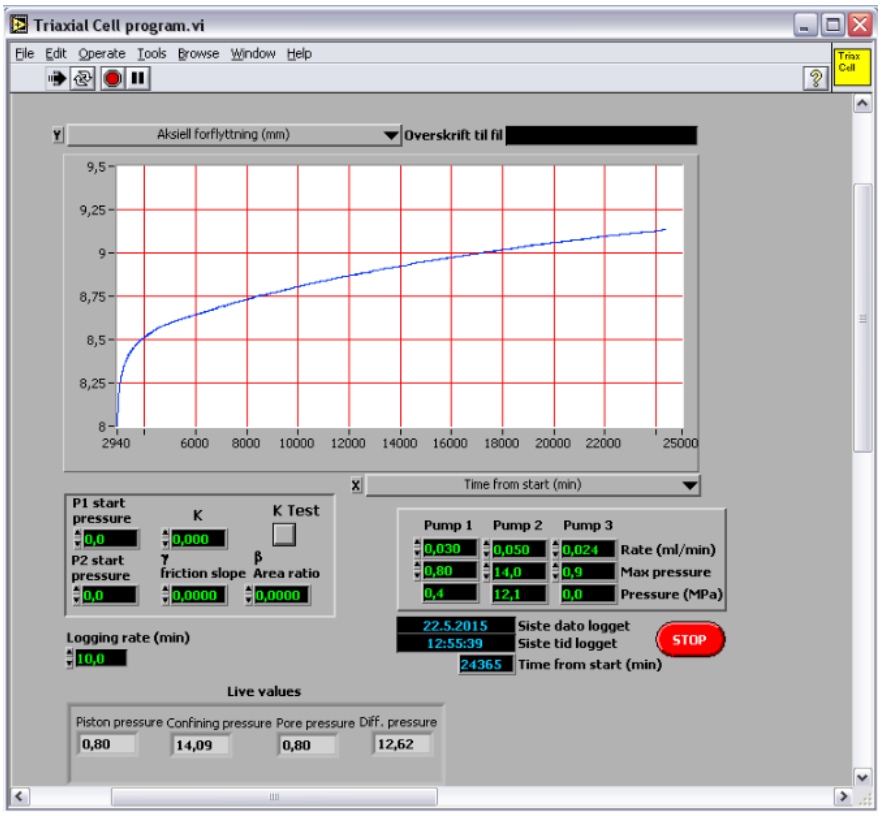

Figure 3.5: *Print screen of the LabView software from the experiment performed on the Mons core M3 at 92° C. This print screen illustrates how LabView can be used to monitor the test by displaying time (min) vs. axial strain (mm) for the first 15 days of creep in the plot.*

3.4 Mechanical Test Procedure

3.4.1 Mounting the Triaxial Cell

The mounting started with the core assembly. The core was mounted between drainage plates on the lower flooding piston on the base of the cell (Fig. 3.6a). Drainage plates were used to allow the fluid flow to intrude the core from several points on the inlet side of the core in stead of only intruding through one point at the center. A shrinking sleeve was placed around the core before the upper flooding piston was placed on top (Fig. 3.6b). The purpose of the sleeve was to prevent the confining oil to intrude into the core during testing. Hence, the sleeve needed to be long enough to cover approximately 1 cm of both the upper and lower flooding pistons. Around the flooding pistons small rubber seals greased with vacuum grease were used to ensure closed system when the sleeve was attached. Heat was applied in order for the sleeve to shrink and tightly cover around the core assembly (Fig. 3.6c). The flooding line from the upper flooding piston was fastened tightly to prevent communication between the brine flooding system and the confining chamber.

The next steps were to fasten the steel cylinder of the confining chamber (Fig. 3.6e), fill the chamber with oil (Fig. 3.6f), attach the heating elements around the chamber (Fig. 3.6g), and put on the piston assembly (Fig. 3.6h). The confining oil used was *Marcol 82* oil. When mounting the steel cylinder and the piston assembly, it was important to ensure that the o-rings were present and that they were in good condition. Six steel bolts were used to mount the parts together (Fig. 3.6i). The bolts ensured that the cell could withstand high pressure during testing. For the experiments with the Mons chalk cores the bolts were tightened with a manually operated torque wrench, while for the experiments with the Kansas chalk cores an electrical torque wrench was used to ensure that the bolts were fasten tight enough to withstand the high confining pressure (24 MPa) used when testing Kansas chalk. The torque setting was 200 Nm. The final step was to attach the LVDT at the top of the piston assembly (Fig. 3.6j).

3.4.2 Start-up Procedure

When the triaxial cell was mounted and pumps, gauges, and all other equipment were connected, the experiments were ready to be started. The start-up procedure lasted for three days and was performed according to the following steps:

Day 1: Confining pressure increased to 0.5 MPa by pumping confining oil at a rate of 2 ml/min. Started core cleaning with distilled water (DW) at a rate of 0.2 ml/min.

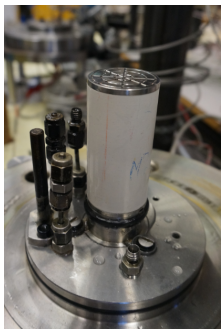

(a) Core placed on lower flooding piston.

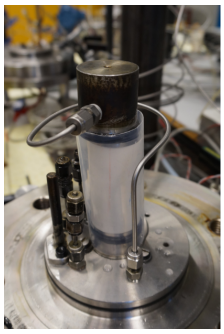

(b) Upper flooding piston mounted.

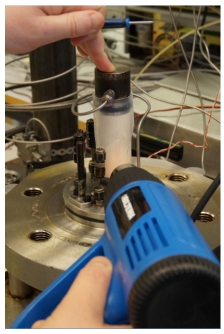

(c) Heat applied on shrinking sleeve.

(d) Sleeve tightly clothed around core.

(e) Fasten steel cylinder.

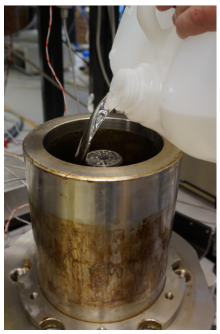

(f) Fill confining chamber with oil.

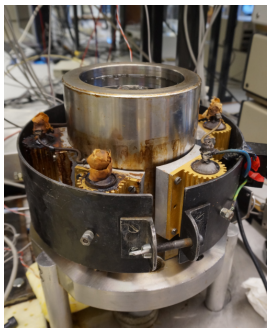

(g) Attach heating elements.

(h) Put on piston assembly.

(i) Mount together cell with steel bolts.

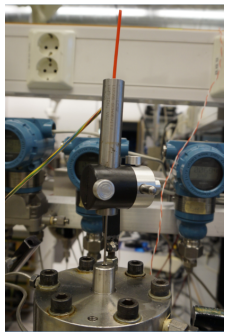

(j) LVDT placed on top of the piston assembly.

Figure 3.6: *Step-by-step pictures of mounting of triaxial cell.*

Day 2:

1. Saturated the core with $MgCl_2$ brine by flooding approximately 1.5 pore volumes (PV's) at a rate of 0.2 ml/min.

2. Confining and pore pressure were built up simultaneously to 1.2 MPa and 0.7 MPa, respectively. A pressure difference of 0.5 MPa was kept during the process by gradually increase maximum pressure limit for the two pumps. Bypass line were open during this process to allow fluid to enter the cores from both sides in order to achieve a more rapid pressure build-up. As pressure increased in the flooding line, the gas pressure supporting the back pressure regulator (BPR) were increased to avoid fluid to come out before a pore pressure of 0.7 MPa was reached.

3. Bypass line was closed to allow flooding through the core.

4. Flooding rate set to 1 PV/day (corresponding to 0.024 ml/min for Mons cores and 0.021 ml/min for Kansas cores).

5. Heating system was turned on. The system was programmed to deliver the desired temperature (60, 92 or 130°). As oil expands during heating, a pressure relief valve was connected to the outlet of the confining chamber. In order to keep the confining pressure constant at 1.2 MPa, the valve was carefully opened or tightened to control the rate of the excess oil that were released. Confining flooding rate was increased and a maximum pump pressure of 1.2 MPa was set to allow confining pressure to build up quickly in case the relief valve was opened to much and pressure would drop below 1.2 MPa.

6. When the desired temperature was achieved, the pressure relief valve was removed and the confining outlet closed.

7. Piston was lowered until contact was established between the piston and the upper flooding piston. This was done by pumping oil into the upper piston chamber, while a bleed off valve was connected to the lower piston chamber to allow excess oil to flow out. The pressure in the upper piston chamber had to overcome a frictional force between the piston and the cylinder in order for the piston to start to move. The pressure needed to initiate the piston movement was the friction pressure (P_{fric}) which was approximately 0.4 MPa for all experiments. To prevent any damage to the core, the maximum piston pressure was set to be 0.3 MPa above the P_{fric}, i.e. ∼0.7 MPa.

Day 3: Start hydrostatic test.

3.4.3 Hydrostatic Test

The hydrostatic test was performed by increasing confining pressure until the creep stress was above the yield point. This process was monitored in LabView where axial movement was plotted against confining pressure in order to serve as a stress-strain plot. If there was observed a absence of axial movement the maximum piston pressure was adjusted. The reason for adjusting maximum piston pressure was because the frictional pressure sometimes increased due to increased confining pressure, causing the piston to get stuck. When the rate of axial deformation started to increase, i.e. the yield point was reached, the loading was continued until the confining pressure was at a value ∼3 MPa higher than yield point before the hydrostatic loading phase was finished. The hydrostatic test performed on Mons chalk were loaded to 14 MPa over 300-500 min, while the test performed on Kansas chalk were loaded to 24 MPa over 500-700 min.

3.4.4 Creep Phase

A creep phase followed the hydrostatic phase. During the creep phase all pressures and rates were kept constant in order for the cores to compact under constant stress and temperature. During the creep phase effluent water was sampled three times a week for Ion Chromatograph (IC) analysis, and twice a week for pH measurements.

3.4.5 Flooding Cell Brine Change Procedure

As the flooding cells only had room for a maximum of 1 liter of $MgCl_2$ brine and the flooding rate was 0.024 ml/day and 0.021 ml/day for Mons and Kansas cores, respectively, the flooding cells had to be refilled a couple of times during the experiments. The refill procedure was performed according to the following steps:

1. Inlet and outlet flooding line into the core were closed, and the bypass line was opened to avoid fluid flow through the core during brine change.

2. Before dismounting the flooding cell from the system, the inlet and outlet valves into the flooding cell were closed and distilled water (DW) bypass line was opened.

3. The flooding cell was lifted to a working table to avoid the triaxial cell to experience any shaking during the brine change. Shaking of the triaxial cell could lead to unwanted movement of the LVDT that registered the axial movement of the core.

4. The valve on the DW chamber was opened to release pressure inside the cell. Seal was opened and DW was poured out until there was only a small volume left. Seal was closed.

5. The piston inside the cell was lifted to give room for new $MgCl_2$ brine in the brine chamber. That was done by injecting air into the brine chamber. To allow the piston to move gently, the DW chamber valve initially was closed before it was slowly opened to release the air. The cell was tilted a little bit with the DW valve pointing upwards to allow all air inside the DW chamber to exit the cell. When water was dripping out of the cell and no more air was coming out, the DW was closed.

6. The flooding cell was turned around to fill up the brine chamber with new brine. The brine valve was opened to release pressure before the seal was opened. Any left-over brine was pored out and the chamber was cleaned with paper. Chamber was filled up with new brine and the seal was closed.

7. The flooding cell was turned around again to have the DW chamber back on top and the cell was lifted back to its position in the experimental set-up.

8. While mounting the flooding cell back to the system, any possible air inside the lines in and out of the cell was removed by flooding through the lines until water was dripping out before the screws was tightened.

9. The flooding cell was pressurized to pore pressure (0.7 MPa) by closing outlet valve and increase flooding rate into the cell.

10. Before the flooding could start through the core, some brine was flooded through the lines to ensure that there was no DW left in the lines between the flooding cell and the core. After a couple of minutes of brine flooding the bypass line were closed, the inlet and outlet line to the core opened, and the brine change was finished.

3.4.6 Dismantling the Triaxial Cell

When the experiment was finished the triaxial cell was dismantled. The dismantling process was performed according to the following steps:

1. The flooding was switched from $MgCl_2$ brine to distilled water (DW) in order to clean the core. DW were flooded for approximate 2-3 days.

2. Temperature system was turned off. As oil shrinks during cooling, the confining pump rate was increased to ensure confining pressure to maintain constant. In addition the piston was lifted in case the core would expand. The lifting of the piston was done by first opening the valve of the upper piston chamber for pressure depletion, and then start pumping oil into the lower piston chamber to push up the piston.

3. During the last phase of temperature decrease, after the temperature had reached about 60°C, the confining pressure was slowly decreased down to 1.2 MPa by stopping the confining pump and opening the confining outlet valve.

4. When the core inside the system reached ambient temperature, the flooding was stopped and the bypass line was opened in order for the pressure to be equal on the inlet and the outlet of the core, i.e. there were no longer any pressure gradient over the core. The gas pressure supporting the BPR was turned off to allow pore pressure to decrease.

5. After pore pressure depletion, the confining pressure was depleted before oil in the confining

chamber was flushed out by injecting air into the inlet of the chamber.

6. The cell was quickly dismantled to avoid the core losing to much water. The cell dismantling process was done in the reverse order of the mounting of the cell (Section 3.4.1). The procedure can be summarized as followed; remove the LVDT, loose and remove the steel bolts, lift up and remove the piston assembly, remove the steel cylinder, loose the flooding line between the upper piston and the bottom of the frame, remove the upper piston, and finally take out the core.

3.4.7 Core Weight and Dimensions Measurements After Testing

When the core was taken out of the cell, it was important to carefully cut the sleeve open and place the core, sleeve and drainage plates on separate storage plates without loosing any chalk pieces. Both the core, sleeve and drainage plates were weighted. Afterwards, all pieces were dried in a furnace at 110°C until all water was evaporated. All pieces were again weighted. The sleeve and the drainage plates were washed free off chalk remains and dried in the furnace. When they were dry, they were weighted. The purpose of this process was to determine total saturated and dry core weight by adding together the weight of the core and the small pieces on the sleeve and drainage plates. Core length and diameter were measured by using a digital caliper on the dry core. Because the core was non-homogeneously deformed, the diameter was measured at intervals at approximately 1 cm along the core. All data needed to calculate new porosity, bulk volume and density was gained.

3.5 Density Analysis

In addition to density determination by the method of comparing dry and saturated core weight, density after testing was also determined by using a gas pycnometer (*Micromeritics Gas Pycnometer AccuPyc II 1340*). This method of density analysis was performed on two Mons chalk cores; M6 (130°C) and M2 (60°C), and one Kansas chalk core; K1 (92°C). As the cores were to big to fit into the measuring cup, the cores were cut into smaller pieces and measured separately. First the cores were cut into two pieces and measured, and later they were further cut into a total of 6 or 7 pieces and measured. The purpose of cutting the cores into 6-7 pieces was to study how density evolved throughout the core from inlet to outlet after testing. Before cutting the core, the flooding direction of each slice was marked with an arrow and the slices were numbered from 1 at the inlet to 6/7 at the outlet. It was important to do this marking to keep control of the relative order and direction of the slices after cutting. Fig. 3.7 shows the Mons core M6 after cutting.

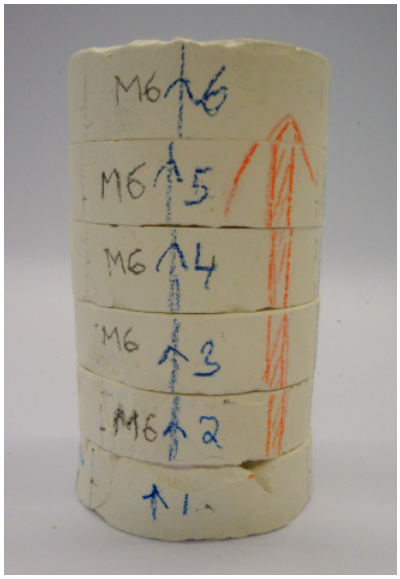

Figure 3.7: *Picture of Mons core M6 (130°C) after cutting into 6 slices. Each slice is marked with an arrow showing the flooding direction and numbered from 1 at the inlet to 6 at the outlet.*

3.6 Ion Chromatography Analysis of Sampled Effluent

From all experiments, the flooding effluent was fractioned approximately three times a week during the entire test period and ion concentration was analysed using a *Dionex ICS-5000$^+$ Ion Chromatograph* (IC). IonPac AS-20 and IonPac CS-19 were used as anion and cation exchange columns, respectively. Prior to the IC analysis, the effluent samples were diluted 500 times with distilled water by using a dilution machine (*Gilson GX-271* and *Hamilton Microlab 600* dilution machines were used). The diluted samples were filtrated through a 0.2 μm filter and transferred into small glass containers. The dilution was done to meet the linear region of the calibration curve of the IC machine. The concentration of the different ions was estimated from the area under the chromatographic curves when compared to known standards. The ion concentration (C_i) was calculated from the following equation,

$$C_i = \frac{A_i}{\overline{A}_{std}} C_{std}$$

where A_i is area under ion curve, $\overline{A}_{std}$ is average area under the standard curves, and C_{std} is the known concentration of the standard. Standards used in this study were synthetic seawater (SSW), calcium magnesium chloride (Ca/Mg/Cl) standard, magnesium chloride ($MgCl_2$) original/refill brine, and distilled water (DW). Salt and ion composition of the standards are listed in Table 3.5.

Table 3.5: *Salt and ion composition of the standards used for Ion Chromatograph analysis.*

Salt	SSW (g/l)	Ca/Mg/Cl (g/l)	$MgCl_2$ (g/l)
NaCl	23.38	0.00	0.00
Na_2SO_4	3.41	0.00	0.00
$NaHCO_3$	0.17	0.00	0.00
KCl	0.75	0.00	0.00
$MgCl_2 \times 6H_2O$	9.05	40.64	44.50
$CaCl_2 \times 2H_2O$	1.91	1.91	0.00
Ion	SSW (mol/l)	Ca/Mg/Cl (mol/l)	$MgCl_2$ (mol/l)
HCO_3	0.002	0.000	0.000
Cl^-	0.525	0.426	0.438
SO_4^{2-}	0.024	0.000	0.000
Mg^{2+}	0.045	0.200	0.219
Ca^{2+}	0.013	0.013	0.000
Na^+	0.450	0.000	0.000
K^+	0.010	0.000	0.000
Ionic strength	0.657	0.639	0.657

3.7 pH Analysis of Sampled Effluent

In addition to ion chromatograph (IC) analysis of the flooding effluent that was measures three times a week, the pH of these effluent samples was also measured using a *Mettler Toledo SevenCompact* pH-meter. These pH measurements were performed several weeks after collecting the effluent. As the effluent samples had been exposed to air and temperature variations due to the IC analysis, there was a suspicion that the pH of these effluent samples might had changed from the time of sampling to the time of pH measurement. Hence, additional effluent samples were collected two times a week and measured continuously for pH analysis. In order to get as good approximation as possible for the pH of the brine when it was flooding inside the core, a minimum volume of effluent brine was collected and the pH was measured right after the sampling finished. The minimum volume of the effluent brine was equal to the minimum volume required for the pH-electrode to be covered with fluid, which in this case turned out to correspond to the collected volume after about 2 hours of sampling into the 8 ml sample glasses.

In order to determine if the pH of the effluent samples changed with time and in that case how much the pH had changed, some effluent samples were sealed and stored in a fridge. Almost daily the samples were taken out of the fridge, heated to ambient temperature and the pH measured.

This procedure was continued until a stable pH value was observed.

3.8 Scanning Electron Microscopy Analysis

To verify the precipitation of new minerals in the chalk matrix after flooding with $MgCl_2$ brine, some of the cores were studied using scanning electron microscopy with X-ray microanalysis (SEM-EDS). The cores used for SEM-EDS study were the two Mons chalk cores M6 (130°C) and M4 (60°C), and the Kansas chalk core K1 (92°C).

Before SEM-EDS analysis the core samples had to be prepared. The cores had been cut into 6-7 slices for the density analysis in the gas pycnometer. For each of the 6-7 core slices in addition to one unflooded chalk slice, a small piece in the flooding direction of the core was cut out for all slices. By doing this it was possible to analyse the whole length of the core from inlet to outlet. The chalk pieces were glued to sample holders and two corners for each sample were marked with conductive carbon cement in order to keep track of the flooding direction. Next step was to coat the samples with a thin layer of carbon in a *Emitech K550 Sputter Coater* machine. This was done to conduct charge away from the chalk surface when the sample was analysed in the SEM machine.

When the samples was finish with coating they were placed inside the SEM machine ready to be analysed. For each sample the measurement started at the inlet flooding side before moving at intervals of 1 mm along the flooding direction of the sample. By doing this the whole core from inlet to outlet at intervals of 1 mm was represented when collecting the data points from all samples.

In order to look for precipitation of magnesite, the SEM was zoomed closely in at the chalk surface and images in addition to EDS measurements were taken when there was observed minerals that had a shape similar to magnesite.

3.9 Failure of Mons Core M2

Mons core M2 failed after 41 days of creep. During the daily monitoring of the experiment, it was observed that the confining pressure had dropped from 14 MPa down to 6.5 MPa during the night, and the differential pressure over the core had increased from about 10 MPa to over 500 MPa in the same time period. The thought was that there must be some leakage inside the system, and the conclusion was that the test had failed. After dismantling the test and inspecting the core, it was confirmed that a leakage was the reason for failure. A small hole was observed in the sleeve at the inlet side of the core above one of the flooding holes in the drainage plate, as seen in Fig. 3.8a,

causing communication between the core and the surrounding confining oil.

(a) *Visible hole in the sleeve at the inlet side of the core.*

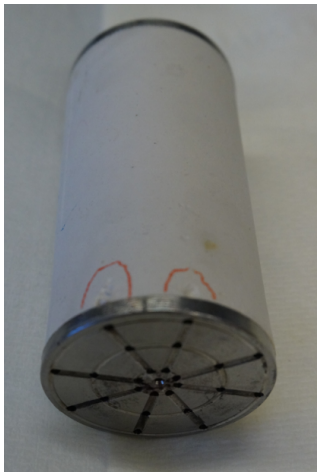

(b) *Core eroded at the edges due to drainage plate holes too far out to the edges.*

Figure 3.8: *Pictures of the Mons core M2 showing the leakage that caused failure of the experiment.*

The reason for the leakage was that the drainage plate that was used had its flooding holes too far out to the edges, causing the chalk to erode in the edges resulting in direct communication between the flooded brine and the sleeve. In Fig. 3.8b the eroded holes are marked with red. This same phenomenon was not seen at the outlet side even though the same type of drainage plate was used there. The learnings from this leakage failure was that drainage plates with flooding holes close to the edges (Fig. 3.9a) only should be used at the outlet side of the core, while for the inlet side, the holes on the drainage plates should be further away from the edges (Fig. 3.9b).

(a) *Flooding holes close to the edge.*

(b) *Flooding holes placed away from the edge.*

Figure 3.9: *Illustration pictures of the different drainage plates.*

4 Results

Results from the mechanical test will be presented first in Section 4.1. The mechanical tests includes the hydrostatic loading phase and the creep phase, and results from Mons and Kansas chalk is presented separately for each phase. In Section 4.2 chemical analysis from ion chromatograph (IC) is presented for three Mons cores and three Kansas cores, one for each temperature (60, 92 and 130°C). Results from mass loss calculations, density estimation from gas pycnometer measurements, and core measurements before and after testing are presented for the three first experiments M6 (130°C), K1 (92°C) and M4 (60°C) in Section 4.3, 4.4 and 4.5, respectively. pH analysis of effluent from all experiments are presented in Section 4.5, and finally the scanning electron microscopy (SEM) analysis of the cores M6, K1 and M4 is presented in Section 4.7

4.1 Mechanical Tests

4.1.1 Hydrostatic Loading

During the hydrostatic loading the cores were loaded hydrostatically to approximately 3 MPa beyond their yield point. This corresponded to a confining pressure of about 14 MPa for Mons cores and 24 MPa for Kansas cores. The results from the hydrostatic loading are presented in stress-strain plots where axial stress is plotted versus axial strain. Yield point was determined by constructing a trend-line to the elastic region and another trend-line to the plastic region. The yield point was found at the intersection of these trend-lines. Bulk modulus was determined as 1/3 of the slope of the trend-line constructed in the elastic region. Since stress was plotted against axial strain and not volumetric strain, the slope of the trend-line was $3K$ when the assumption of isotopic condition was used ($\varepsilon_{vol} = 3\varepsilon_{ax}$). The results for Mons and Kansas cores are presented in separate subsections below.

Mons Cores: A stress-strain plot for all four Mons cores are presented in Fig. 4.1 and yield point and bulk modulus are presented in Table 4.1. From the plot, it can be observed that all graphs start out with differences in the slopes in the beginning, but that they yield at approximate the same value between 11.7-12.0 MPa. M2, which was tested at 60°C, was stiffer than the other cores with a steeper graph in the beginning compared to the other graphs, i.e. M4 had a higher bulk modulus of 1.21 GPa compared to values in the range of 0.92-1.02 GPa for the other cores. M2 and M3 were both tested at 92°C, and it can be observed that the graphs for these cores have a similar shape. This result in similar values for yield points of 11.71 and 11.83 MPa and bulk modulus

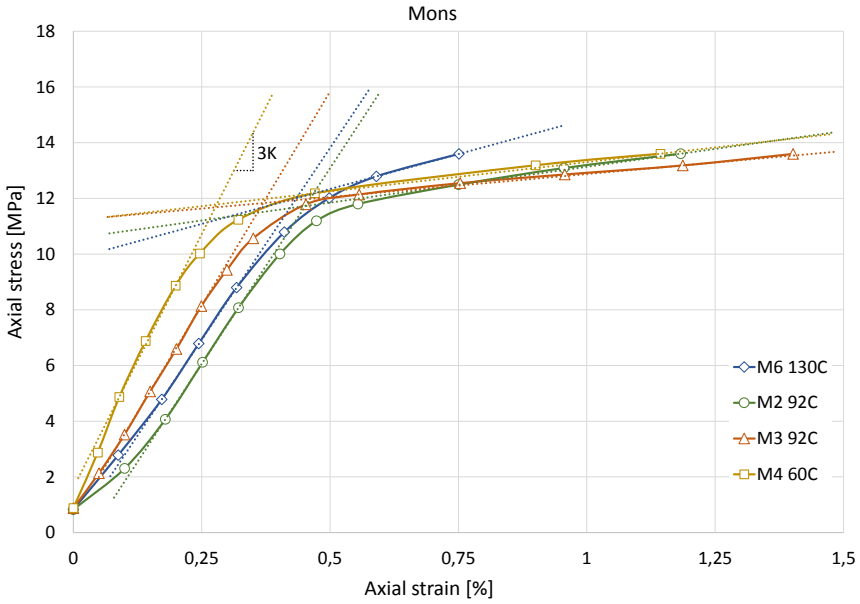

Figure 4.1: *Axial stress versus axial strain for Mons cores. M4 was stiffer than the other cores, i.e. it had the highest bulk modulus. M2 and M3, both tested at 92°C had similar behaviour with yield points of 11.7 and 11.8 MPa and bulk modulus of 0.94 and 1.02 GPa, respectively.*

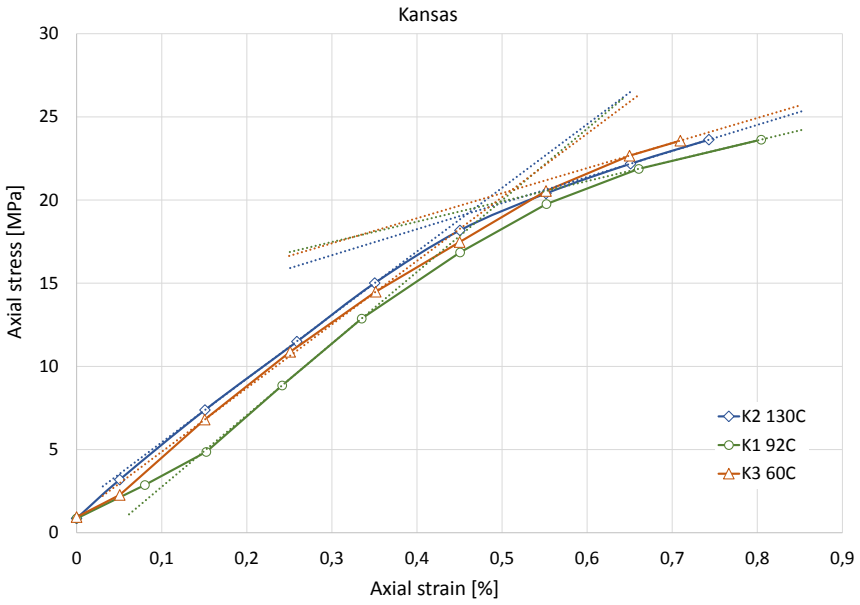

Figure 4.2: *Axial stress versus axial strain for Kansas cores. All Kansas cores behaved similar during hydrostatic loading with yield points ranging from 18.7 to 20.6 MPa and bulk modulus ranging from 1.27 to 1.44 GPa.*

of 0.94 and 1.02 GPa for M2 and M3, respectively.

Table 4.1: *Yield point and bulk modulus of Mons cores.*

Core	Testing temperature	Yield point [MPa]	Bulk modulus [GPa]
M6	130°C	12.00	0.92
M2	92°C	11.72	0.94
M3	92°C	11.83	1.02
M4	60°C	11.78	1.21

Table 4.2: *Yield point and bulk modulus of Kansas cores.*

Core	Testing temperature	Yield point [MPa]	Bulk modulus [GPa]
K2	130°C	19.18	1.27
K1	92°C	18.67	1.44
K3	60°C	20.57	1.28

Kansas Cores: A plot of axial stress versus axial strain for all four Kansas cores are presented in Fig. 4.2 and yield point and bulk modulus is presented in Table 4.2. From the plot, it can be observed that the graphs matches relatively good. Yield points and bulk modulus are relatively similar, ranging from 18.7 to 20.6 MPa and 1.27 to 1.44 GPa, respectively.

4.1.2 Creep Phase

Mons Cores: Plot of axial creep strain versus creep time for Mons cores are presented in Fig. 4.3. Creep data for Mons cores M2 and M3 until 60 days of creep phase is not available as M2 failed after about 40 days and M3 was started up after the M2 failure and therefore is still running. It can be observed that the graph for M6, which was tested at 130°C, stands out from the other graphs. The creep curves for the cores tested at 60 and 92°C are very similar. They had a high deformation rate the first couple of days during the creep phase. Axial strain increased by about 1% in 2 days and after that the deformation rate gradually eased off throughout the test. M4, that are the only one of these cores that was tested for 60 creep days, ended up with an axial creep strain of 2.1%. Similar to the other cores M6 also had a high deformation rate in the beginning, but M6 did not deform as much as the other cores. M6 deformed 0.6% during the first 2 days. After that the axial strain stabilized and was almost constant until the deformation rate started accelerating at 20 days of creep. From this time, M6 deformed in a much higher rate than the other cores. At about 35 days, M6 were passing the other cores in axial creep strain and at the end of the creep phase at 60 days, the axial creep strain was 3.1%.

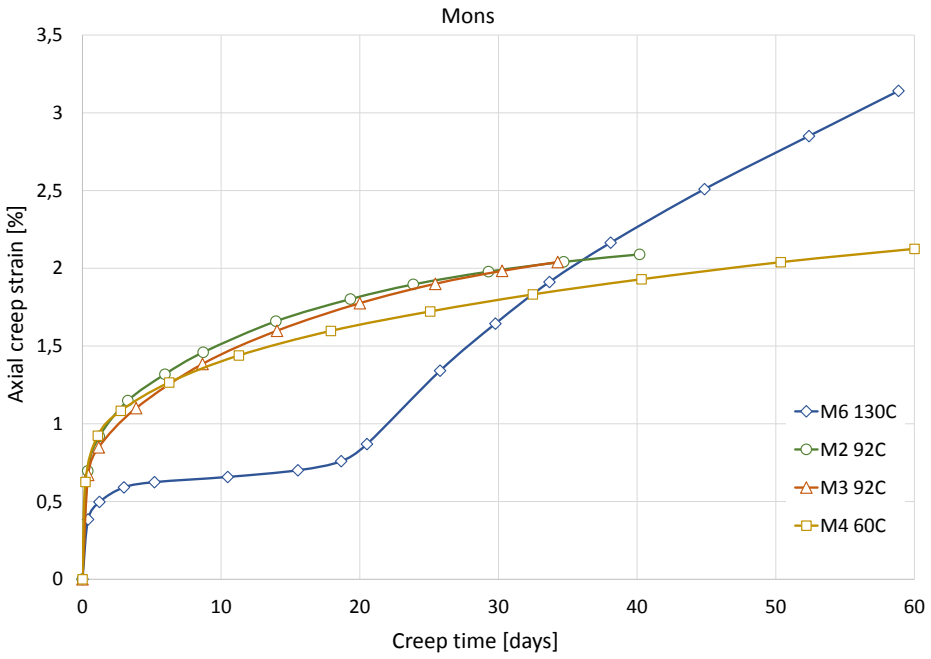

Figure 4.3: *Axial creep strain versus creep time for Mons cores. Note that M6 tested at 130°C had a lower deformation rate than the cores tested at lower temperatures during the first 20 creep days. At 20 days, M6 deformation rate accelerates resulting in a higher creep strain than the other cores. M2, M3 and M4 showed similar behaviour.*

Permeability was calculated during testing according to Eq. 2.25 for all experiments. Permeability for Mons cores is plotted together with axial creep strain against creep time in separate plots in Fig. 4.4. By studying the plots, the permeability and the creep strain seems to be related to each other. For all cores the permeability slowly decreases when creep strain increases. When axial creep strain is almost constant for M6 between day 2 and 20 (Fig. 4.4a), the permeability graph takes a small shift to the right before starting to decrease again when creep strain starts accelerating, i.e. the permeability seems to stabilize for a short time during the time when axial strain was constant. In total the permeability for M6 decreased from 3 to 0.5 mD.

There are two observations in the plots for M3 and M4 (Fig. 4.4c and Fig. 4.4d, respectively) that do not fit with the just mentioned observation of permeability being related to creep strain. The first observation is that the permeability for M3 has a relatively big decrease from 1.9 to 0.8 mD the first creep day before decreasing with a more reasonable rate onwards. At 20 creep days the permeability makes a jump from 0.7 to 0.8 mD before continuing the slow decrease ending up at 0.5 mD at 35 days, which was the last day of available data. The other observation is that the permeability for M4 fluctuated more than the other cores (M2, M3 and M6). The permeability

had some fluctuations while it decreased from 1.1 to 0.7 mD. There was an unexpected increase at around 22 and 48 creep days where the permeability increased by about 0.1 mD. Permeability for M2 (Fig. 4.4b) had a relative stable decrease from 1.2 to 0.9 mD during the 40 days of creep.

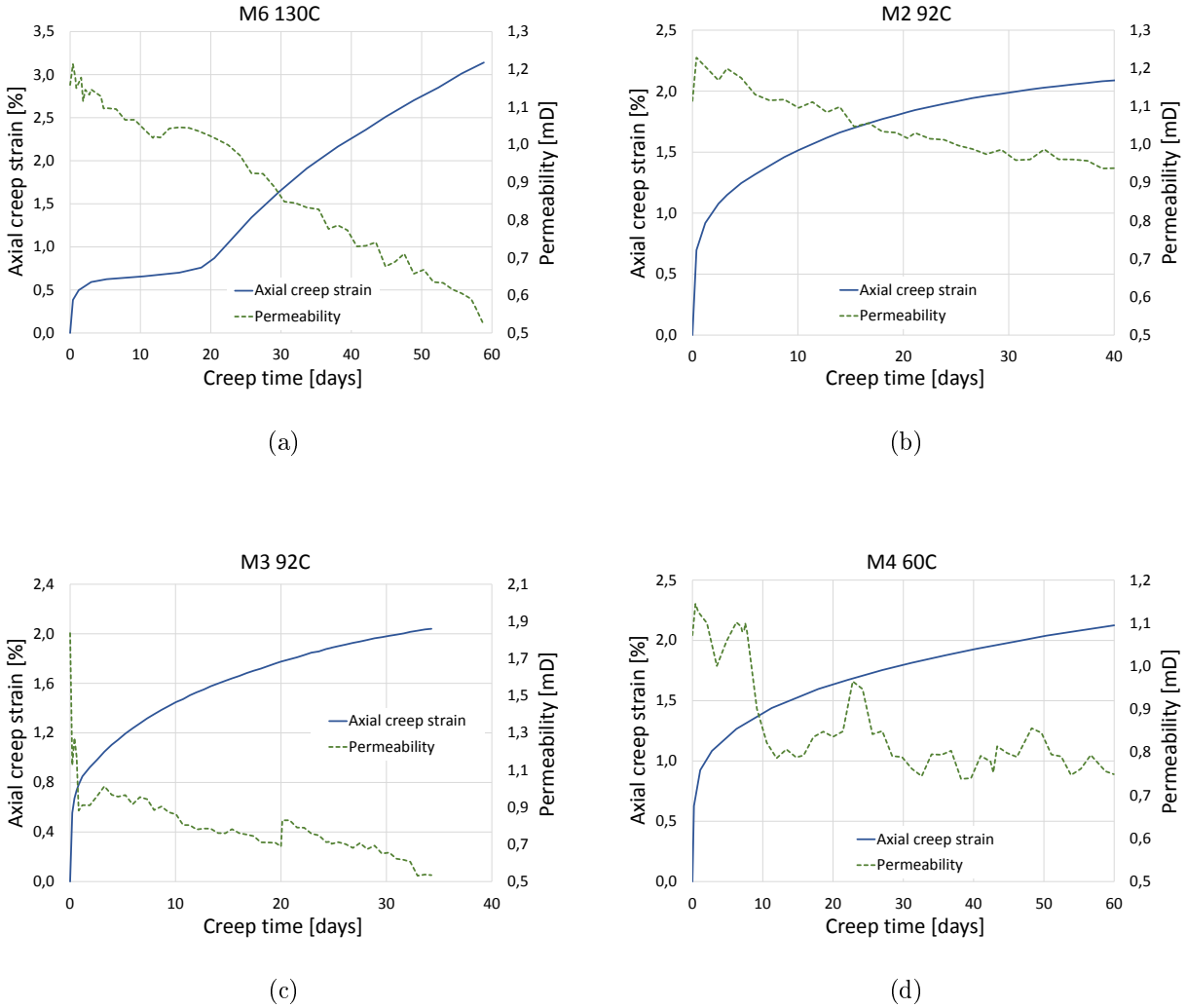

Figure 4.4: *Axial creep strain and permeability plotted against creep time for Mons cores. Note that permeability decreases with increasing axial creep strain. (a) The permeability of M6 stabilizes for a short time between 10 and 20 creep days when creep strain is almost constant. (b) M2 had a gradually decrease from 1.2 to 0.9 mD throughout the creep phase. (c) M3 had a significant permeability drop from 1.9 to 0.8 mD the first creep day, and gradually decreased from that point and throughout the test except for a jump of 0.1 mD at 20 creep days. (d) Permeability of M4 decreases from 1.1 to 0.7 mD with fluctuations.*

Kansas Cores: Plots with axial creep strain versus creep time for Kansas cores are presented in Fig. 4.5. Similar as for the creep curve plot for the Mons cores (Fig. 4.3), the core tested at 130°C shows a different behaviour than the core tested at lower temperatures. All cores had a high deformation rate with an axial creep strain of about 0.5% during the first day of creep before deformation rate started easing off. For K1 and K3, tested at 92 and 60°C respectively, deformation rate stayed relatively constant throughout the test resulting in a total axial creep strain of 1.3% for K3 and 1.7% for K1. For K2 tested at 130°C, on the other hand, an accelerating creep behaviour was observed after 10 days. After 60 days, K2 had a total axial creep strain of 2.6%.

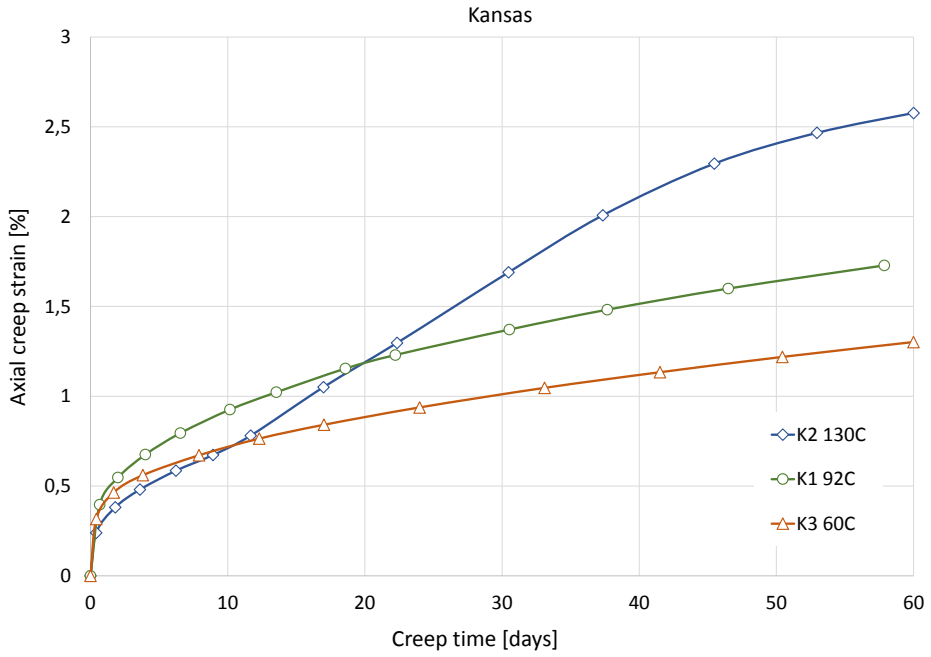

Figure 4.5: *Axial creep strain versus creep time for Kansas cores. All core show similar creep behaviour in the beginning, but at 10 creep days the deformation rate of K2, tested at 130°C, accelerate bypassing the creep strain of the other cores. Not that total creep strain increase with temperature.*

Permeability is plotted together with axial creep strain against creep time for the Kansas cores in separate plots in Fig. 4.6. Similar as to the Mons cores the permeability decreases as the creep strain increases in the beginning, but later in the creep period the permeability curves for all cores shows some unexpected fluctuations. The permeability of K2 dropped from 1.4 mD to almost zero the first 22 days and stayed that low throughout the test (Fig. 4.6a). The permeability of K1 (Fig. 4.6b) decreased from 0.8 to 0.3 mD the first 20 creep days. At 20 days the permeability made a jump of about 0.2 mD before it slowly decreased again. At creep time 50 days, the same happened again; permeability made a jump of 0.2 mD before it decreased slowly. When the test ended at 60 creep days the permeability of K1 was 0.4 mD. For K3, the permeability decreased from

1.2 to 0.6 mD throughout the creep test (Fig. 4.6c) At around 45 creep days the permeability makes a jump of 0.1 mD at.

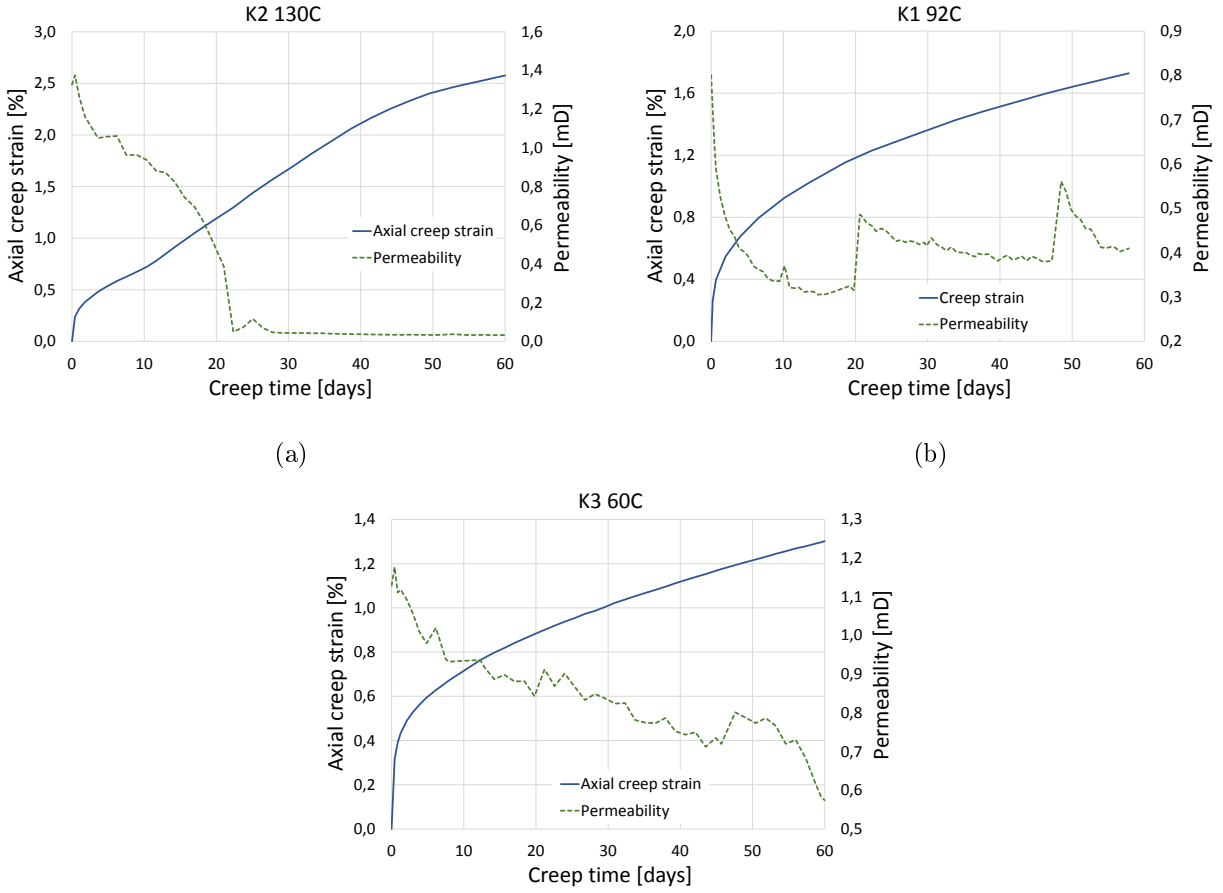

Figure 4.6: *Axial creep strain and permeability plotted against creep time for Kansas cores. Permeability decreases with increasing axial creep strain. (a) The permeability of K2 was 1.4 mD at time 0 and gradually decreased the first creep days before it dropped to almost zero at 22 days and stay low throughout the test. (b) The permeability of K1 was 0.8 mD at time 0 and had a decreasing trend throughout the test except at creep day 20 and 50 where the permeability made a jump of approximately 0.2 mD. (c) The permeability of K3 had a gradually decrease from 1.2 to 0.5 mD throughout the test, with one jump in permeability of 0.1 mD at time 45 days.*

4.2 Chemical Analysis of Sampled Effluent

Effluent water was analysed in an Ion Chromatograph (IC) for all cores except Mons core M3, which was the new experiment performed on 92°C after M2 failed. The results from the IC analysis for each core are presented in plots of ion concentration of chloride, magnesium and calcium plotted against creep time of the effluent samples in Fig. 4.7. In addition to the ion concentrations, there is one "Mg+Ca"-curve that summarizes the magnesium and calcium concentration in each point. The dashed lines with long dashes illustrates the original chloride concentration in the injected $MgCl_2$ brine, and similar the dashed line with shorter dashes illustrates the original magnesium concentration. For all cores the chloride concentration in the effluent was about 0.438 mol/l, which is equal to the original chloride concentration in the injected $MgCl_2$ brine. Also the "Ca + Mg"-curve matches the original magnesium concentration of 0.219 mol/l relatively good for cores.

From the results gained from core M6 (Fig. 4.7a), tested at 130°C, it can be observed that the the magnesium concentration generally was lower in the effluent samples compared to the original concentration of the brine throughout the tests. For M6, magnesium concentration was 0.177 mol/l in the first effluent sample compared to the original brine concentration of 0.219 mol/l magnesium. The magnesium concentration increased to about 0.2 mol/l during the first 10 days of creep and stabilized at that level throughout the test. There was no calcium in the injected $MgCl_2$ brine. Hence, the observed calcium concentration in the effluent samples indicates that calcium was dissolved from the chalk matrix. The calcium concentration was 0.041 mol/l in the first effluent sample. Over the next 10 days of creep the calcium concentration decreased to about 0.02 mol/l and stabilized at that level throughout the test. The curves for magnesium and calcium are mirroring each other.

Kansas core K2, tested at 130°C , had similar results as M6 (Fig. 4.7b). The first effluent samples had a magnesium concentration of 0.170 mol/l and a calcium concentration of 0.036 mol/l. Over the next 6 creep days, magnesium increased to a concentration of about 0.193 mol/l and calcium decreased to 0.025 mol/l and both ions stayed constant at those levels throughout the test. Similar as for M6, the curves for magnesium and calcium for K2 are mirroring each other.

For the cores M2 and K1 (Fig. 4.7c and 4.7d, respectively), both tested at 92°C, the magnesium and calcium concentration was more or less stable in the effluent throughout the creep phase. For both cores, magnesium concentration was between 0.210 and 0.214 mol/l and calcium concentration was 0.004 and 0.009 mol/l in the effluent throughout the test.

For the cores M4 and K3 (Fig. 4.7e and 4.7f, respectively), both tested at 60°C, ion concentrations in the effluent samples was very close to the original concentrations of the brine. The curve for magnesium concentration matched the original magnesium concentration curve for both cores.

Calcium concentration in the effluent was stable around 0.002 mol/l for M4 and 0.003 mol/l for K3.

4.3 Calculation of Mass Loss

Total mass loss in core M6 (130°C), K1 (92°C) and (60°C) was calculated as described in Section 2.2.6. Concentration and mass changes for each species and total mass loss is presented in Table 4.3. Magnesium values have negative sign because magnesium is precipitated in the core, while the positive sign of calcium and carbonate means that the species have dissolved from the core. For all cores, the carbonate concentration in the effluent was almost zero. M6 had the highest magnesium precipitation of 0.040 mol and the highest calcium dissolution of 0.045 mol. As magnesium has a lower weight than calcium, M6 also had the largest mass loss of 1.10 g. The measured mass loss from weight difference of dry weight before and after testing was 1.41 g for M6. Magnesium precipitation and calcium dissolution for K1 was 0.009 and 0.012 mol, respectively, resulting in a total mass loss os 0.44 g compared to the measured mass loss of 0.96 g. M4 had almost zero magnesium precipitation and calcium dissolution of 0.003 mol and 0.002 mol, respectively, resulting in a total mass loss of 0.30 g. M4 had a measured mass loss of 0.67 g.

Table 4.3: *Integrated magnesium and calcium concentrations from IC-data for the cores M6, K1 and M4, tested at 130, 92 and 60°C, respectively. A positive sign means that the effluent has a higher concentration than the injected brine. The additional* Ca^2 *concentration compared to* Mg^2 *concentration indicated dissolution of* CO_3^{2-}.

	M6 130°C	K1 92°C	M4 60°C
$\Delta n(Mg^{2+})$ [mol]	-0.040	-0.009	-0.003
$\Delta n(Ca^{2+})$ [mol]	0.045	0.012	0.005
$\Delta n(CO_3^{2-})$ [mol]	0.005	0.003	0.002
$\Delta m(Mg^{2+})$ [g]	-0.97	-0.23	-0.08
$\Delta m(Ca^{2+})$ [g]	1.79	0.49	0.23
$\Delta m(CO_3^{2-})$ [g]	0.28	0.18	0.15
Δm_{tot} IC-data [g]	1.10	0.44	0.30
Δm_{tot} Measured [g]	1.41	0.96	0.67

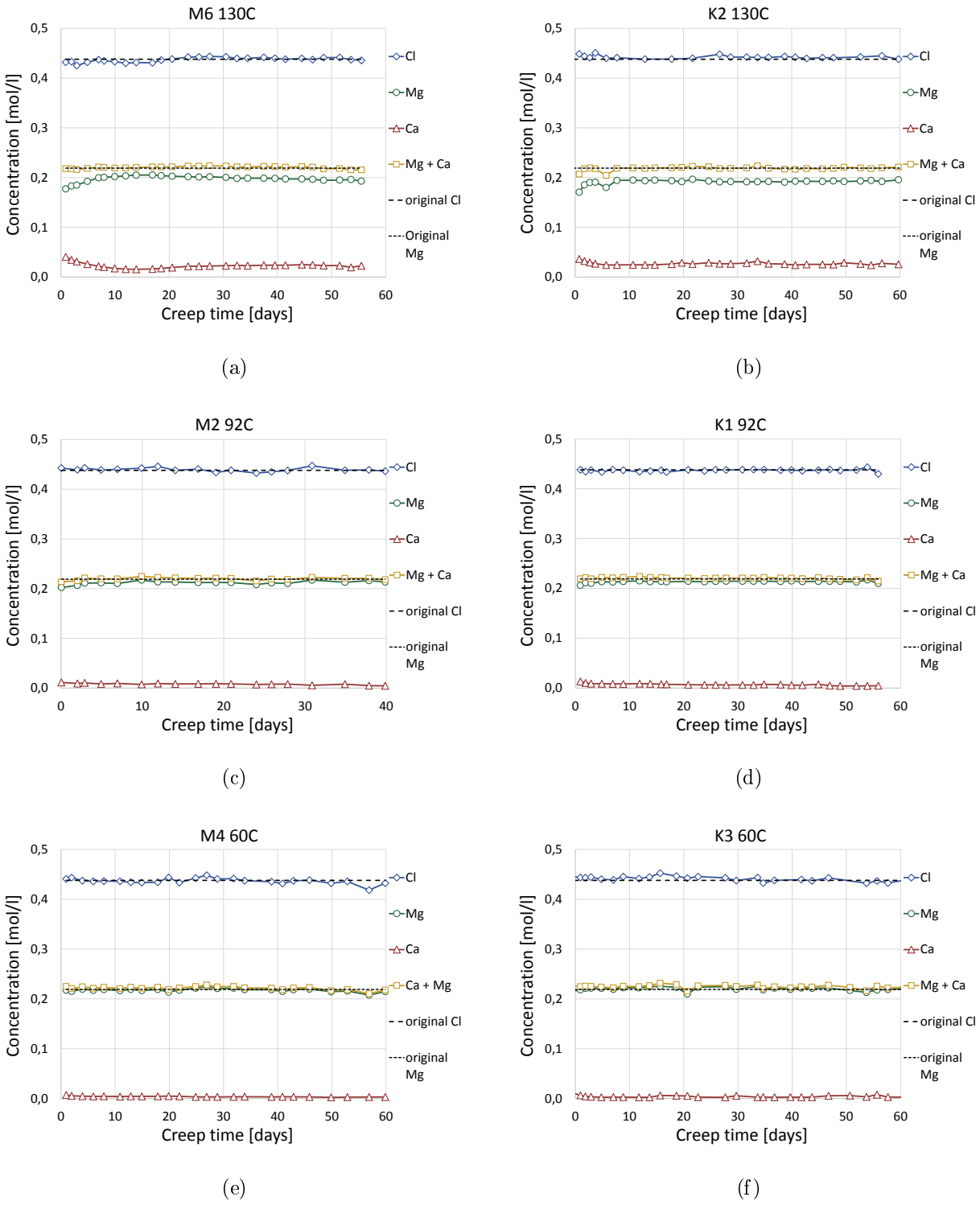

Figure 4.7: *Results from IC analysis showing the ion concentration of chloride, magnesium and calcium in effluent water samples plotted against creep time. Dashed lines illustrate original chloride (long dashes) and magnesium (short dashes) in the injected* $MgCl_2$ *brine. "Ca+Mg"-curve summarize magnesium and calcium concentration for each point. The difference between the injected and produced concentrations increases with increasing temperature.*

4.4 Density Measurements from Gas Pycnometer

The density of the Mons cores M6 (130°C) and M4 (60°C) and the Kansas core K1 (92°C) were analysed in a gas pycnometer. First the cores were cut into two pieces, which were labeled *big inlet piece* and *big outlet piece*, before measured in the gas pycnometer. Further the two big pieces were cut into smaller pieces resulting in a total of six or seven small pieces, which were labeled *small pieces* from *1* at the inlet side to *6* at the outlet side. Weighted average density was measured according to Eqs. (2.15) and (2.16).

M6 130°C: Table 4.4 presents the results from the density analysis of the Mons core M6, tested at 130°C. When only one small piece was measured in the gas pycnometer, a warning was given from the machine that the volume inside the chamber was low which can give errors in the results. Hence, some of the small pieces were measured together to reduce the uncertainty of big errors. Two different methods of measuring the small pieces were used. The small piece *1* was measured first, and afterwards all the other small pieces from *2* to *6* were measured together. In the next round two and two pieces were measured together; *1-2*, *3-4* and *5-6*.

The results show that there are differences in average density when measuring big and small chalk pieces. And there are also a difference in the results between the two methods used to measure the small pieces. Big pieces had an average density of 2.72 g/cm^3. The first method on the small pieces gave 2.71 g/cm^3, while the second method gave 2.70 g/cm^3. Original density of M6 was calculated to be 2.96 g/cm^3 according to Eq. (2.14). Thus, all density estimations from gas pycnometer measurements indicate that the density increased during testing.

Table 4.4: *Density calculations from gas pycnometer analysis of M6 tested at 130°C. The core was first cut into two big pieces and measured before it was cut further into smaller pieces and measured by combining the small pieces together by two different ways. Weighted average density is measured from each method.*

	Piece name/nr.	Density [g/cm^3]	Avg. Density [g/cm^3]
Big pieces	Inlet piece	2.72	2.72
	Outlet piece	2.72	
Small pieces method 1	1	2.73	2.71
	2-6	2.71	
Small pieces method 2	1-2	2.70	2.70
	3-4	2.70	
	5-6	2.69	

K1 92°C: Table 4.5 presents the results from the density analysis of the Kansas core K1, tested at 92°C. In addition to the tested core, two unflooded chalk pieces were measured in the gas pycnometer. The unflooded pieces were end pieces of K1 that were cut off during preparation of the core before testing. The end piece that was cut off from the inlet side was labeled *unflooded inlet piece* and the piece that was cut off from the outlet side was labeled *unflooded outlet piece*.

The results show that the average density of the unflooded pieces is 2.70 g/cm^3, which is equal to the original density of K1 calculated according to Eq. (2.14). The average density of both the big pieces and the smaller pieces is 2.71 g/cm^3. Hence, the density might had increased somewhat during testing.

Table 4.5: *Density measurements gas pycnometer analysis of K1 tested at 92°C.*

	Piece name/nr.	Density [g/cm^3]	Avg. Density [g/cm^3]
Unflooded pieces	Inlet piece	2.70	2.70
	Outlet piece	2.70	
Big pieces	Inlet pieces	2.71	2.71
	Outlet piece	2.71	
Small pieces	1	2.72	2.71
	2	2.70	
	3	2.69	
	4	2.70	
	5	2.71	
	6	2.71	
	7	2.72	

M4 60°C: Table 4.6 presents the results from the density analysis of the Mons core M4, tested at 60°C. Simialr as for K1, unflooded chalk pieces of M4 were measured. The results show that both unflooded pieces and the tested big and small pieces had a average density of 2.70 g/cm^3.

4.5 Core Measurements Before and After Testing

Because the core M2 failed and the experiments on the cores M3, K2 and K3are still running, the core measurements of the cores M6 (130°C), K1 (92°C) and M4 (60°C) are the only ones to be compared before and after testing in this section. Bulk volume, porosity and density calculations are performed as described in Section 2.2.5. For porosity calculations from method 3 (Eq. (2.13)), the average density was estimated from the gas pycnometer measurements of the big core pieces,

Table 4.6: *Density measurements gas pycnometer analysis of M4 tested at 60°C.*

	Piece name/nr.	Density [g/cm^3]	Avg. Density [g/cm^3]
Unflooded pieces	Inlet piece	2.69	2.70
	Outlet piece	2.70	
Big pieces	Inlet pieces	2.70	2.70
	Outlet piece	2.70	
Small pieces	1	2.71	2.70
	2	2.70	
	3	2.70	
	4	2.70	
	5	2.70	
	6	2.71	
	7	2.70	

i.e. after cutting the cores into two pieces. The results from M6, K1 and M4 are presented in Table 4.7, 4.8 and 4.9, respectively.

M6 130°C: During testing, bulk volume of M6 decreased by about 5.4 cm^3. This reduction was caused by compaction and permanent deformation of the core, which also were visible when looking at the core after testing. Fig. 4.8 shows a picture taken of M6 after testing where the core deformation that had taken place during testing clearly can be observed. Flooding direction is marked by an arrow, and it can be seen that the diameter is smallest at the inlet side of the core and increases towards the outlet side, i.e. the deformation was greatest at the inlet side. The same significant deformation difference between inlet and outlet side of the core was not observed for K1 and M4, which were tested at 92 and 60°C, respectively. Density and porosity calculations for M6 agree with the observed compaction. Density increased from 2.69 to 2.72 g/cm^3 during testing based on density calculations from Eq. 2.14. A density of 2.72 g/cm^3 was also found according to Eqs. (2.15) and (2.16) when the gas pycnometer measurements of the big half pieces (Table 4.4) was used. Porosity after testing was calculated to be 39.6% from method 1 and 3 and 38.2% from method 2 compared to an original porosity of 42.2%. Method 1 and 3 gives the same result since the density calculations from Eq. (2.14) and Eqs. (2.15) and (2.16) was equal.

K1 92°C: K1 had a reduction in bulk volume of 3.8 cm^3 during testing. Density increased from 2.70 to 2.71 g/cm^3 according to Eq. (2.14). Calculated average density from gas pycnometer for the big core pieces also gave 2.71 g/cm^3. Hence, porosity calculation from method 1 and 3 gave an

Figure 4.8: *Picture of Mons core M6 showing permanent deformation after testing. The arrow indicate flooding direction during testing.*

equal result of 34.0%. Porosity from method 2 was calculated to be 33.3%. Original porosity was 36.5%.

M4 60°C: M4 had a reduction in bulk volume of 4.4 cm^3 during testing. Density increased from 2.70 to 2.71 g/cm^3 according to Eq. (2.14). Density estimations according to Eqs. (2.15) and (2.16) from the gas pycnometer measurements of the big core pieces gave a density of 2.70 g/cm^3, i.e. equal to original density. Porosity calculation from method 1, 2 and 3 gave 39.7%, 39.2% and 39.6%, respectively. Original porosity was 42.5%.

Table 4.7: *M6 core measurements before and after testing.*

	Before testing	After testing
Bulk volume [cm^3]	82.07	76.69
Density [g/cm^3]	2.69	2.72
Porosity (Method 1) [%]	42.2	39.6
Porosity (Method 2) [%]	-	38.2
Porosity (Method 3) [%]	-	39.6

Table 4.8: *K1 core measurements before and after testing.*

	Before testing	After testing
Bulk volume $[cm^3]$	81.04	77.25
Density $[g/cm^3]$	2.70	2.71
Porosity (Method 2) [%]	36.5	34.0
Porosity (Method 2) [%]	-	33.3
Porosity (Method 3) [%]	-	34.0

Table 4.9: *M4 core measurements before and after testing.*

	Before testing	After testing
Bulk volume $[cm^3]$	82.58	78.17
Density $[g/cm^3]$	2.70	2.71
Porosity (Method 1) [%]	42.5	39.7
Porosity (Method 2) [%]	-	39.2
Porosity (Method 3) [%]	-	39.6

4.6 pH Analysis of Sampled Effluent

The pH of the effluent samples that was measured minutes after sampling are presented in Fig. 4.9. As the pH was measured straight after sampling, it indicated the pH inside the core during testing. For both Mons and Kansas cores it can be observed that the pH was in the range 5.5-6.5 for all cores. The pH is fluctuating up and down with time. It is not certain if this fluctuation was actual or if it was due to uncertainties in the pH meter.

For Mons cores (Fig. 4.9a), M6 that was tested at 130°C generally had the lowest pH starting off with a pH of about 6 that decreased to about 5.6 at 25 creep days and stayed around that value throughout the test. M2 and M3, both cores tested at 92°C, had a pH of about 6.4 through the whole creep phase. M4, tested at 60°C, had a pH of 6.2 the first 20 days, a pH of 6 the next 25 days, and the last days 10 days the pH increased to above 6.5.

For Kansas (Fig. 4.9b), also the core tested at 130°C generally had the lowest pH of about 5.8. K1, tested at 92°C, had a similar behaviour as M4. The pH was around 6.1 the first 20 days, below 6 the next 30 days, and during the last days the pH increased up to 6.8. K3, tested at 60°C, had a pH fluctuation around 6.3 throughout the test.

The pH of the effluent samples that were used for IC analysis is presented in Fig. 4.10. The effluent samples were measured several weeks after they were sampled. For both Mons and Kansas cores the

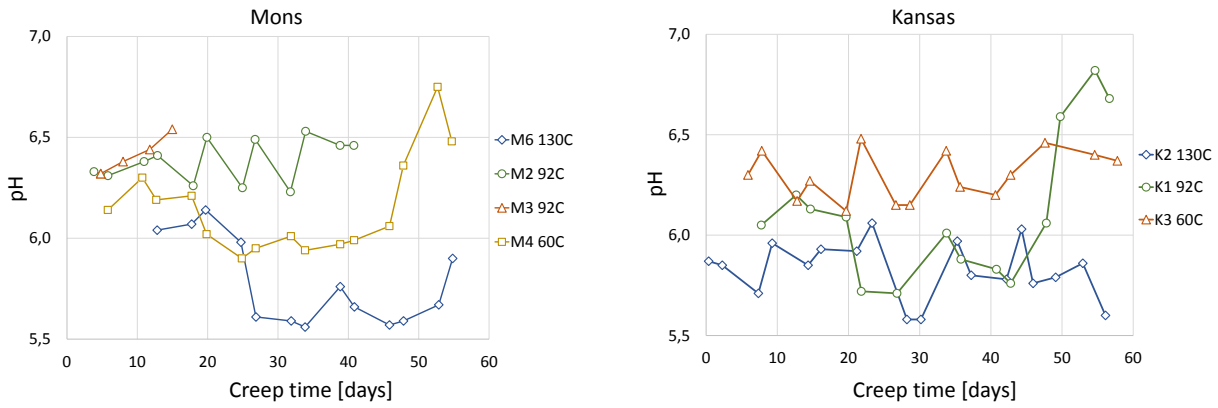

(a) (b)

Figure 4.9: *Measured pH of effluent samples from Mons (a) and Kansas (b) cores during testing. pH was measured minutes after sampling and is in the range of 5.5-6.5 for all cores. Note the fluctuating pH.*

effluent samples had a pH of almost 8, which means that the pH increases with a value of almost 2 when comparing the effluent samples that where measured minutes after sampling and these older samples. From the plots it can be observed that the pH was relatively stable for each core. M6 had pH values around 7.7 and K1 and M4 around 7.9. These results agree with the results from the analysis where the pH of the same effluent samples was measured almost daily until a stable pH value was observed. In that study, effluent samples from M6, M4 and K1 were analysed. It was observed that the pH for all cores had a pH of about 6 the first day of measurement, and that the pH increased up to about 8 within approximately 2-3 weeks.

4.7 SEM Analysis

Three cores were analysed by SEM; M6 tested at 130°C, K1 tested at 92°C and M4 tested at 60°C. The results from the SEM-EDS analysis were plotted as weight percentage (wt%) of total collected components for each data point. As the data points were selected with an interval of 1 mm in the flooding direction of each chalk sample, the core from inlet to outlet is represented in the plots when all data points is plotted together in correct order. It is important to state that these plots cannot be used to determine exact amount of the different components of the chalk. The reason is that the plots only present weight percentage of the components that was chosen to be collected by the SEM machine. There are minerals that are not accounted for during the SEM analysis. In this study the plots are used to look at the trend of the magnesium wt% in order to get an indication of the magnesium amount in the tested cores. The first data points in each plot are analysis of unflooded

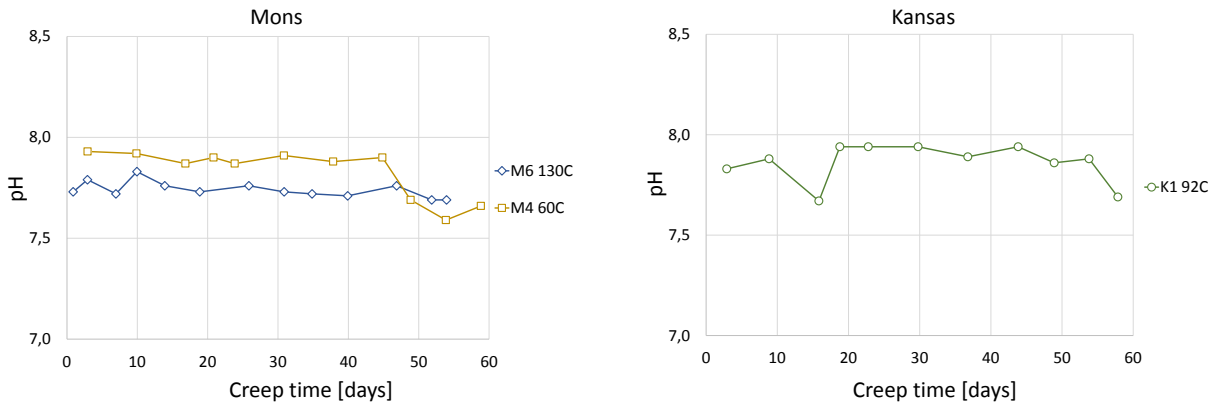

(a) (b)

Figure 4.10: *Measured pH of effluent samples that were used for IC analysis from Mons (a) and Kansas (b) cores. The pH was measured several weeks after sampling. pH of M6 was stable around 7.7, while pH of M4 and K1 was stable around 7.9.*

chalk pieces that was cut off the inlet and outlet of the cores prior to testing.

M6 130°C: The SEM-EDS results from Mons core M6 are plotted in Fig. 4.13, where Fig. 4.13a presents weight percentage of all the collected components, while Fig. 4.13b presents magnesium weight percentage alone. The first nine data points in both plots are analysis of unflooded M6 chalk pieces. Data point nr. 10 is at the inlet of M6, and the last point is at the outlet. From the plot with magnesium plotted alone, it can clearly be seen that the weight percentage of magnesium is significantly higher in the tested M6 core compared to the unflooded chalk. Unflooded chalk had 0.3 wt% magnesium, while the highest magnesium amount in the core was measured to be 1.8 wt% about 2 cm into the core from inlet side. The magnesium amount was higher at the inlet side and decreased towards the outlet. From the plot with all components together, it can be observed that calcium had an increasing trend from inlet to outlet of the core.

By zooming into the chalk surface of M6 and studying it more closely, magnesite precipitation was detected by the inlet side of the core. SEM images and EDS analysis of detected magnesite are presented in Fig. 4.11. When magnesite was analysed by EDS, the number of X-rays count of magnesium and oxygen was high. As comparison, in the chalk texture around the magnesite, the magnesium peak was low and calcium was the dominating peak. Apart from the precipitated magnesite it was not observed any other significant differences in the matrix texture of the tested chalk and the unflooded chalk.

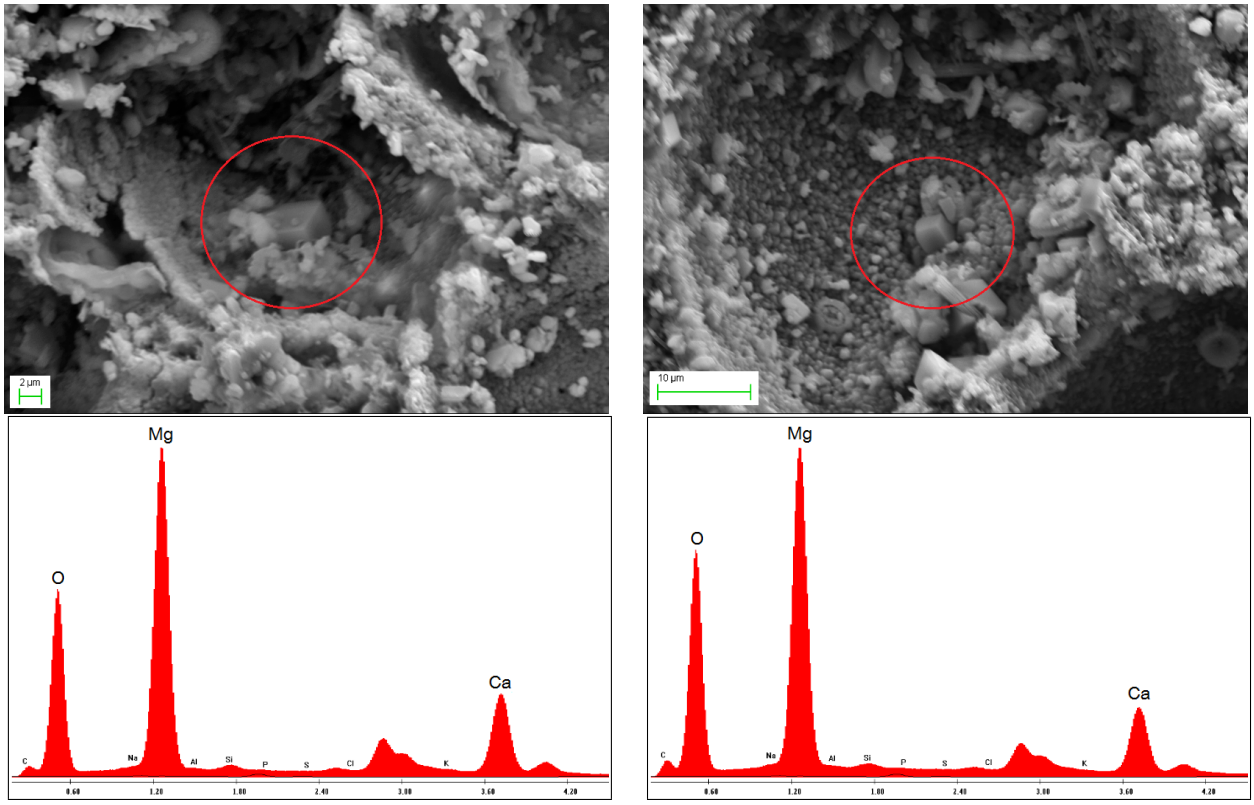

Figure 4.11: *SEM images of Mons core M6 (tested at 130° C) showing precipitation of magnesite (marked by red circles) after flooding with* $MgCl_2$. *Associated EDS analysis are presented in graphs as number of X-ray counts versus energy level of X-rays below the images and are showing large amount of magnesium and oxygen.*

K1 92°C: The SEM-EDS results from Kansas core K1 are plotted in Fig. 4.14. The first six data points are analysis of unflooded chalk. Unflooded chalk had a magnesium amount of approximate 0.3 wt%. The trend in Fig. 4.14b, that presents magnesite plotted alone, indicates that the weight percentage of magnesium was highest by the inlet with a weight percentage of 0.7 and decreased towards the outlet ending up with a value of about 0.4 wt%, which is almost the same amount measured in unflooded chalk.

No evidence of magnesite was found in K1, but anhydrite was detected (Fig. 4.12). No significant difference in the matrix texture of the tested chalk and the unflooded chalk was seen.

M4 60°C: The SEM-EDS results from Mons core M4 is plotted in Fig. 4.15. The first three data points are the analysed unflooded chalk. When studying Fig. 4.15b, it can be observed that only the inlet side of the core (from data point nr. 4 to 15) had a higher weight percentage of magnesium compared to the unflooded chalk. The highest magnesium amount was measured to

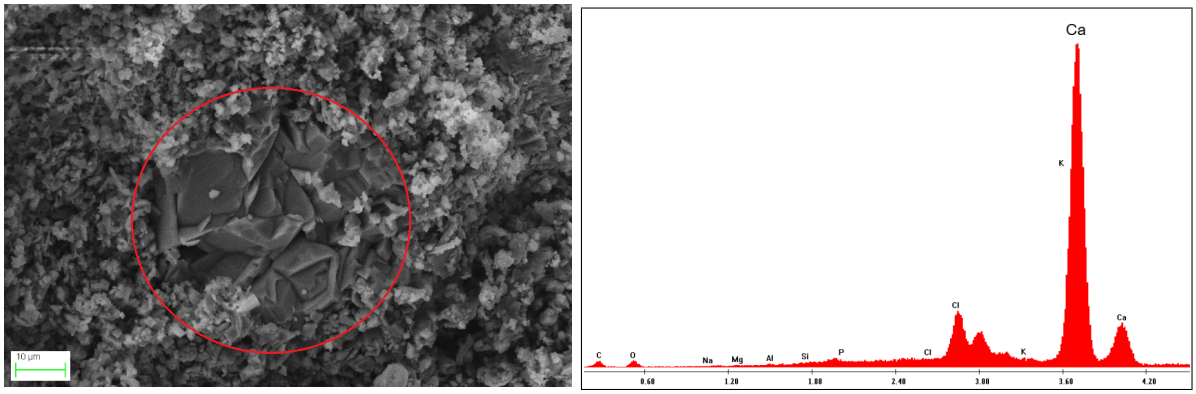

Figure 4.12: *SEM images of Kansas core K1 (tested at 92°C) showing precipitation of anhydrite (red circle) after flooding with* $MgCl_2$. *EDS analysis show a big amount of Ca.*

be approximately 0.6 wt%. After data point 15 the magnesium weight percentage was equal to unflooded chalk ranging between 0.2 and 0.3.

There was not found any evidence of magnesite in M4, and there was no significant difference in the matrix texture when comparing the tested core and unflooded chalk.

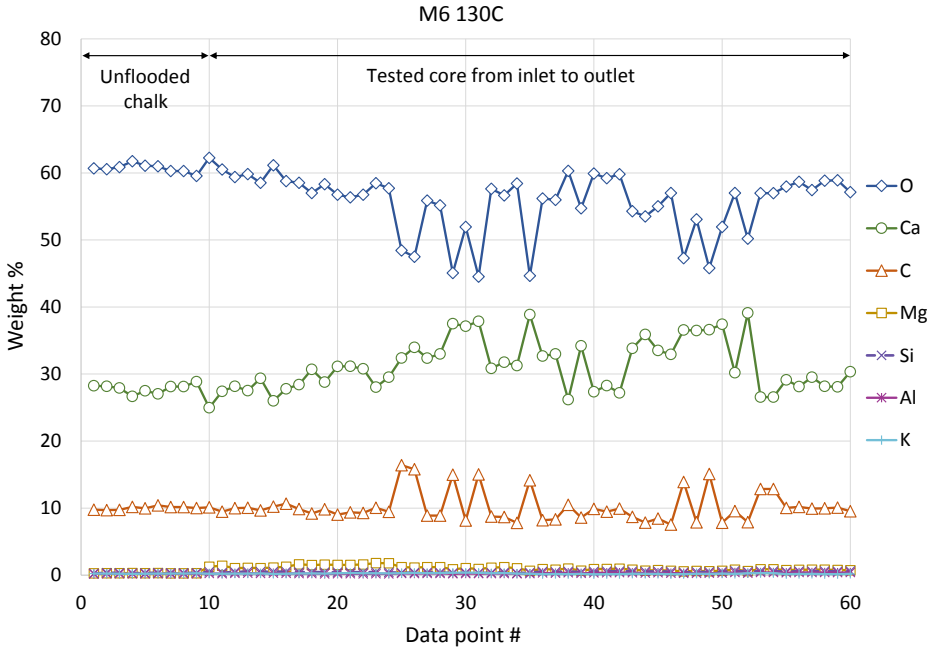

(a)

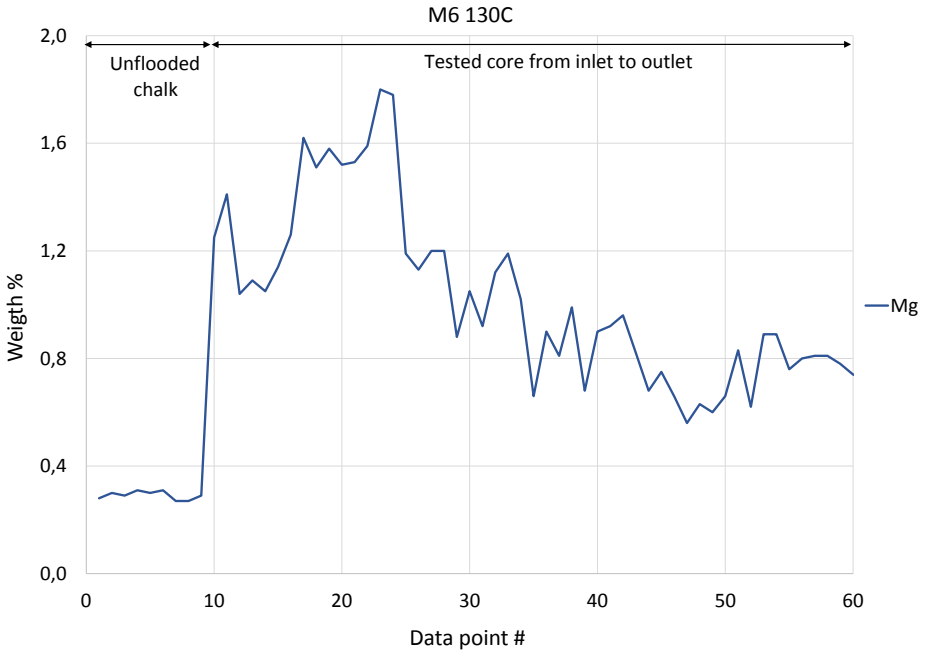

(b)

Figure 4.13: *Components plotted as weight percentage of total amount of collected components in the SEM-EDS analysis for Mons core M6 tested at 130° C. The first nine data points are analysis of unflooded chalk. (a) Weight percentage of calcium show an increasing trend from inlet to outlet of M6. (b) Wight percentage of magnesium in the core was for all data points higher than the unflooded chalk that had a value of 0.3 wt%. Highest wt% of magnesium was measured about 2 cm into the core from inlet side (data point 23). Weight percentage of magnesium decreased to 0.8 throughout the core.*

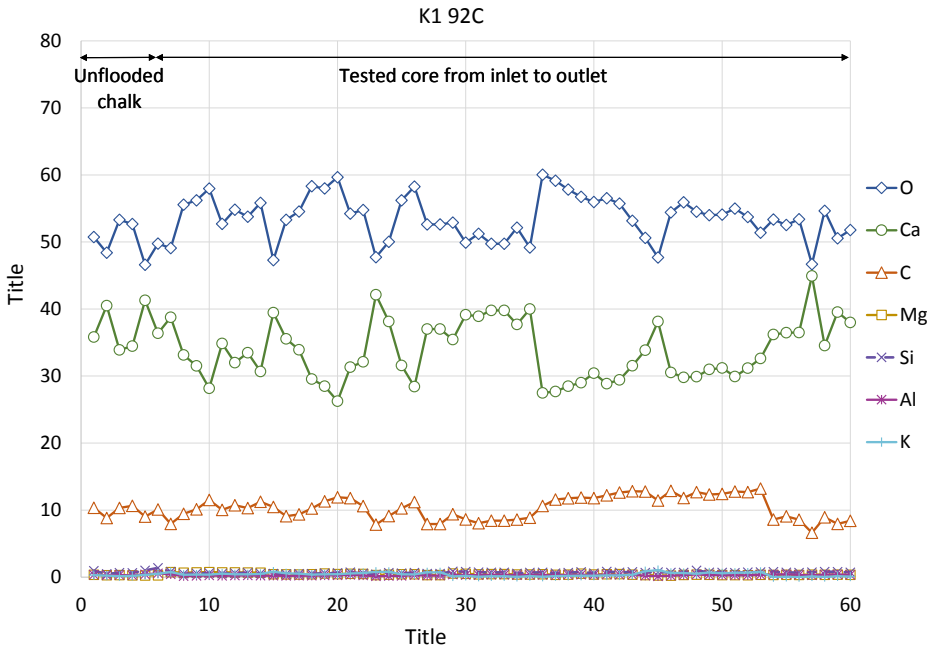

(a)

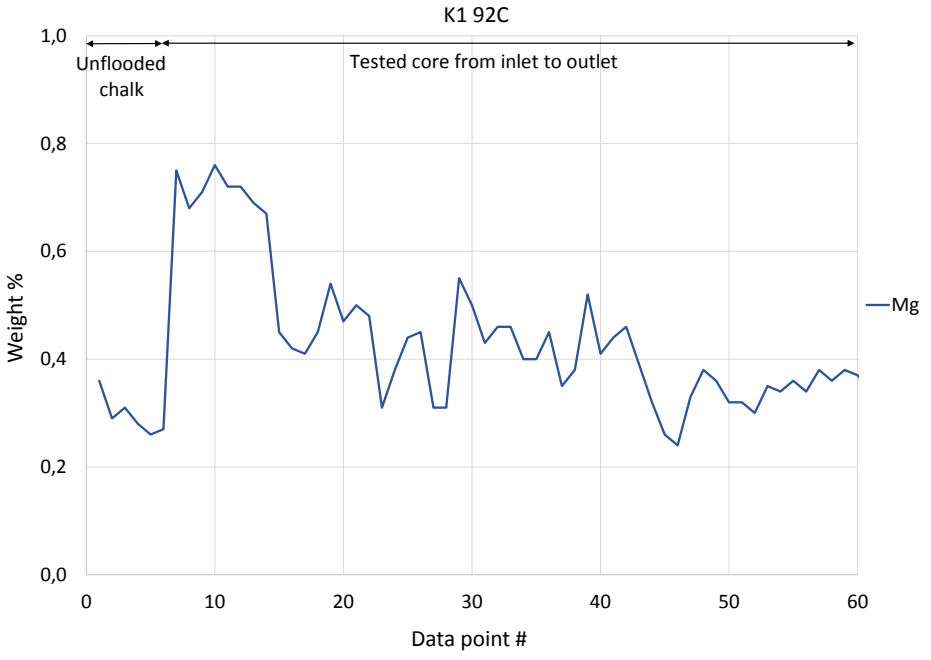

(b)

Figure 4.14: *Components plotted as weight percentage of total amount of collected components in the SEM-EDS analysis for Kansas core K1 tested at 92° C. The first six data points are analysis of unflooded chalk. Highest wt% of magnesium at the inlet of the core with a value of 0.7. Magnesium wt% decreased throughout the core to 0.4 wt%, which was approximately same wt% magnesium measured in unflooded chalk.*

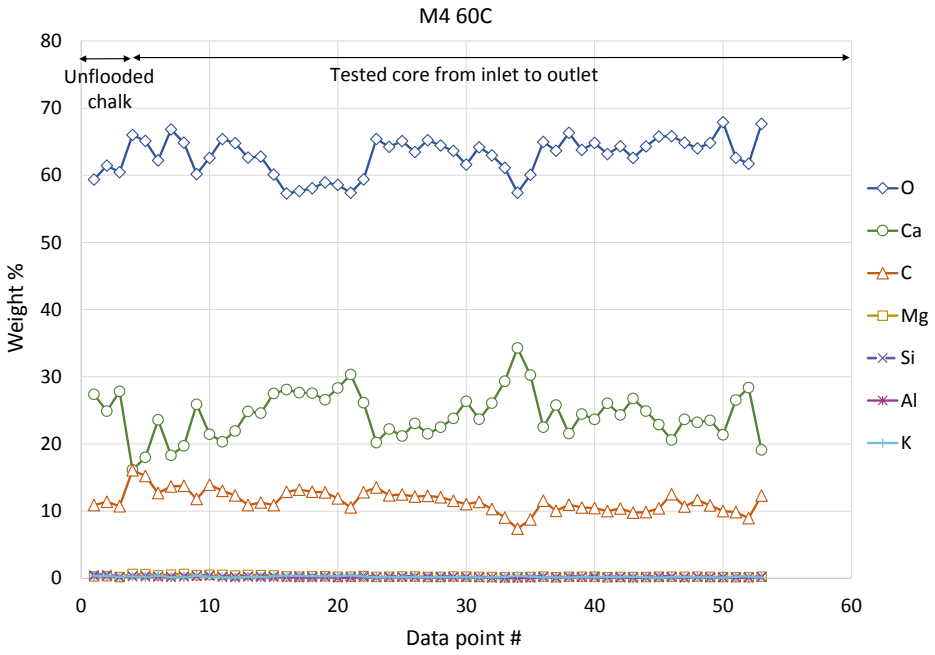

(a)

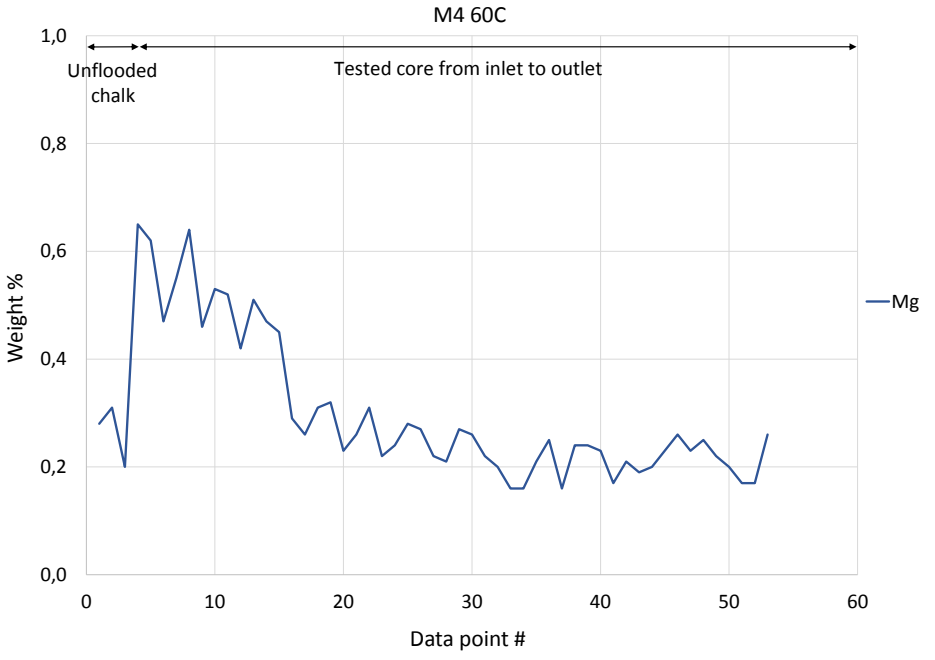

(b)

Figure 4.15: *Components plotted as weight percentage of total amount of collected components in the SEM-EDS analysis for Mons core M4 tested at 60° C. The first three data points are analysis of unflooded chalk. Only the inlet of the core had higher magnesium weight percentage than unflooded chalk, with highest magnesium weight percentage of 0.6. Unflooded chalk had 0.3 wt% magnesium.*

5 Discussion

5.1 Effect of Temperature During Mechanical Tests

No significant temperature effects was observed for Kansas cores during hydrostatic loading. Kansas cores behaved more or less the same, with similar yield point and bulk modulus (Fig. 4.2, Table 4.2). Axial strain at the end of the hydrostatic loading was in the range of 0.7-0.8%, i.e. relatively equal. During the creep phase, on the other hand, higher axial strain was observed with higher temperature. Total axial strain is plotted against creep time in Fig. 5.1. Total axial strain of K2 (130°C) was lower than the other Kansas cores (K1 92°C and K3 60°C) during the first creep days, but as creep started accelerating after about five days the total axial strain of K2 shortly bypassed the other cores ending up at 3.3%, corresponding to a creep strain of 2.6%. For comparison, the total axial strain for the core tested at 60°C (K3) ended at of 2.0% and the core tested at 92°C (K1) ended at 2.6%, which correspond to a creep strain of 1.3 and 1.7%, respectively.

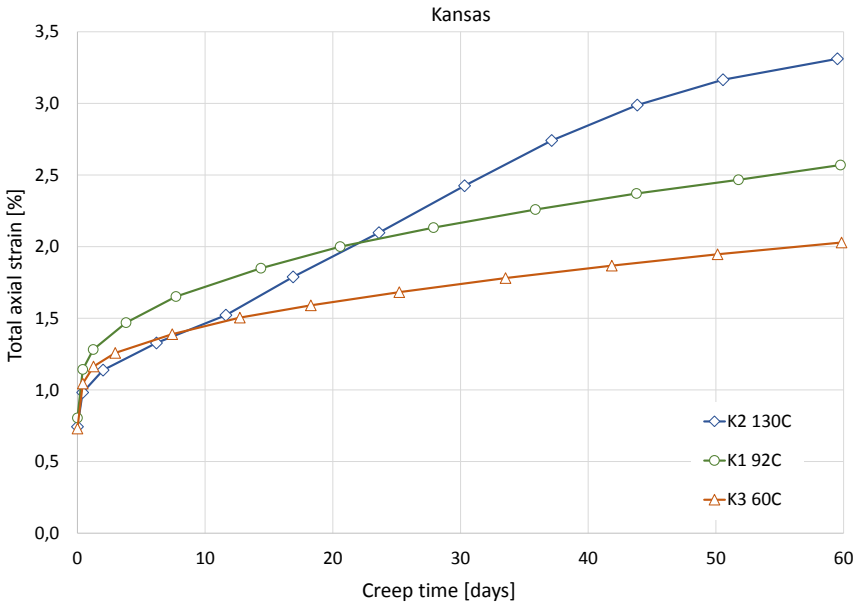

Figure 5.1: *Total axial strain versus creep time for the Kansas cores. Note that there seem to be a temperature dependency of the strain in the end of the creep phase.*

For the Mons cores there were observed some minor differences during hydrostatic loading (Fig. 4.1). There seems to be a trend towards lower bulk modulus with increasing temperature. M4, tested at 60°C, had a higher bulk modulus than the Mons cores tested at 92 and 130°C. Two Mons cores was tested at 92°C, and those had different bulk modulus. Hence, the differences in the bulk modulus can be a result of small variations in rock properties of the cores and not necessarily due

to the temperature. Before concluding if there are a temperature dependency or not for Mons chalk during hydrostatic loading, more additional experiments should be performed to confirm the results from this study. But it should be mentioned that previous tests have been showing good repeatability for this type of chalk, i.e. Mons chalk (Megawati et al., 2015; Tobiesen, 2013). During hydrostatic loading there was a clear difference in axial strain for the Mons core tested at 130°C (M6) compared to the cores tested at 60°C (M4) and 92°C (M2 and M3) (Fig. 4.1). M6, tested at 130°C, had an axial strain of 0.75% in the end of the hydrostatic loading, while the other Mons cores had a higher axial strain of 1.1-1.4%.

The difference in the axial strain for M6 compared to the other Mons cores became more significant when the creep phase started. In Fig. 5.2 total axial strain is plotted against creep time for the Mons cores. It can be observed that M6 (130°C) started out with the lowest total axial strain of 0.75% when the creep phase started and it also had the lowest total axial creep strain over the first ten creep days. For comparison, the other Mons cores (M2, M3 and M4) had a total axial strain in the range of 2.54-2.86% after the first creep days. Hence, in addition for M6 to compact less than the other Mons cores during hydrostatic loading, it also compacted less than the other cores in the beginning of the creep phase. At 130°C Mons chalk seems to better withstand compaction than at lower temperatures until the point where creep strain starts accelerating. Due to the acceleration, the creep strain of M6 (130°C) exceeded the other Mons cores (M2 and M3 at 92°C and M4 at 60°C) resulting in a total axial strain of 3.9% after 60 days, corresponding to a creep strain of 3.1%. As data for M2 and M3 (both tested at 92°C) is not available after 40 and 34 creep days, respectively, the total axial strain is extrapolated from the data up until 60 days (Fig. 5.2). From Fig. 5.2 it is estimated that total axial strain of Mons cores tested at 60 and 92°C (M2, M3 and M4) ends at approximately 3.9-3.3% after 60 days, corresponding to a creep strain in the range of 2.1-2.4%. This indicates that at 60 days the total axial strain is actually not that different between all four Mons cores, but it should be noted that the core tested at 130°C (M6) had a significantly higher deformation rate at 60 days compared to the cores tested at lower temperatures.

Between the core tested at 60 and 92°C (M2, M3 and M4) there was no significant difference in the compactional behaviour during creep strain (Fig. 5.2). When comparing the extrapolated axial strain of M2 (92°C) with the axial strain of M4 (60°C), the strain difference seem to be constant with time. When comparing the extrapolated axial strain of M3 (92°C) with the axial strain of M4, on the other hand, the difference between the strain increases with time indicating a temperature dependency of compaction. More experiments on Mons chalk should be perform to determine if there is a temperature difference of strain between 60 and 92°C.

For both Mons and Kansas cores the highest creep strain was observed for the cores tested at 130°C. Same results were observed by Nermoen et al. (under review) when they performed similar

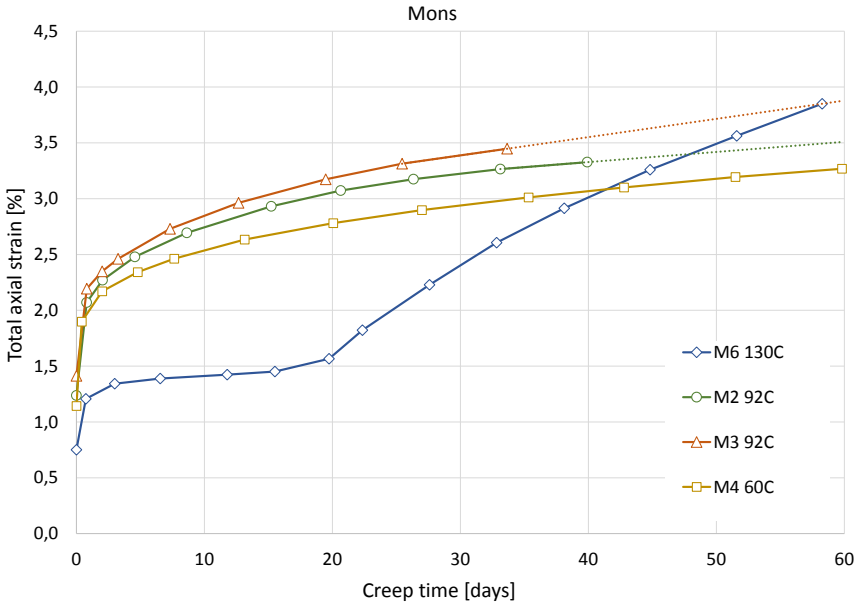

Figure 5.2: *Total axial strain versus creep time for the Mons cores where the strain for M2 and M3 is extrapolated until 60 days. Note that the strain difference between M2 (92°C) and M4 (60°C) is more or less constant, while the difference between M3 (92°C) and M4 increases with time.*

experiments on outcrop chalk from the Obourg quarry in the Saint Vast formation in Belgium. They flooded the cores with $MgCl_2$ at 130 and 92°C at different effective hydrostatic stress levels (0.5, 3.5 and 12.5 MPa). For each stress level, the cores tested at 130°C had the highest compaction. Similar as for the experiments performed in this thesis, accelerating creep was observed for 130°C, but not for the cores tested at 92°C. In the studies of Nermoen et al. (under review), accelerating creep was only significant for the cores tested with an effective stress of 3.5 and 12.5 MPa. Accelerating creep behaviour has also been observed by other researchers (Madland et al., 2011; Megawati et al., 2015) on both Mons and Stevns Klint chalk flooded with $MgCl_2$ at 130°C. Madland et al. (2011) performed experiments on Stevns Klint cores with two different pore pressures; 0.7 and 40 MPa, and they only observe accelerating behaviour when the cores were flooded with $MgCl_2$ at a pore pressure of 40 MPa, and not on 0.7 MPa. For the experiment performed on Mons chalk at 130°C and 0.7 MPa in this thesis, accelerating creep was observed after about three weeks. Mons and Stevns Klint are both very pure chalks with similar properties (Megawati et al., 2015). Hence, as Madland et al. (2011) stopped the experiments after two weeks, there are reason to believe that creep would have started accelerating also for the Stevns Klint core after a prolonged time.

As accelerating creep was observed for the cores tested at 130°C after some days of steady state creep, it have been discussed if maybe accelerating creep also will be observed on similar experiments on lower temperatures when they are run for sufficiently long time. Hence, the objective of running

the last three experiment over longer time instead of stopping them after 60 creep days was to see if accelerating creep would be observed also for the cores tested at lower temperatures. One Mons core is still running at 92°C and two Kansas cores are still running; one at 60°C and the other at 130°C. Although it was observed an accelerating creep on the Kansas core at 130°C after about ten creep days, that experiment is still running to observe the further creep behaviour over a prolonged time. The exact reason behind the accelerating creep behaviour is not understood today, and a question that is still unanswered is; can more than one accelerating creep phase be observed over time at constant temperature, pressure and flooding rate?

5.2 Effect of Chalk Type in Mechanical Tests

As mentioned in the previous section, the compaction of the Kansas cores was observed to behave similar at the different temperatures during hydrostatic loading and in the beginning of creep phase, while the Mons core tested at 130°C (M6) compacted less than the Mons cores tested at lower temperatures (M2, M3, and M4). After some days of creep phase, the deformation rate for M6 almost stopped before the accelerating creep started. Megawati et al. (2015) had the same observations when they flooded different chalk types (Mons, Stevns Klint, Kansas, Aaborg and Liège) with $MgCl_2$, NaCl and DW at 130°C. While the creep strain of the impure chalk cores (Kansas, Aaborg and Liège) flooded with $MgCl_2$ was seen to increase to a level 2-4 times higher than those flooded with NaCl and DW, the pure chalk cores (Mons and Stevns Klint) flooded with $MgCl_2$ had a significantly lower axial creep in the beginning of the creep phase. The results showed that creep enhancement of pure chalks when flooded with $MgCl_2$ compared to non-reactive fluids does not occur from initial time. The pure chalks had a delayed enhanced creep response that was not seen for the impure chalks. Megawati et al. (2015) discussed this difference in terms of the content of non-carbonates in the impure chalks which are chemically altered immediately. They suggested that non-carbonate phase present in chalk were supporting the grain structure. Hence, the immediate dissolution of non-carbonates caused the chalk to compact. As non-carbonates are almost non existing in pure chalk, this immediate compaction was not seen. The accelerating creep was by Megawati et al. (2015) suggested to be a result of time dependent calcite dissolution.

Axial stress versus axial strain during hydrostatic loading for Mons and Kansas cores if plotted together in Fig. 5.3, and total axial strain versus creep time is plotted for Mons and Kansas cores in Fig. 5.4, where dashed lines are Mons cores and solid lines are Kansas cores. The results and the suggested mechanism by Megawati et al. (2015) matches well with the results of the tests performed on 130°C for both Mons and Kansas in this thesis (M6 and K2), but it cannot explain why the Mons cores tested at 60 and 92°C (M2, M3 and M4) did have a significantly higher compaction rate

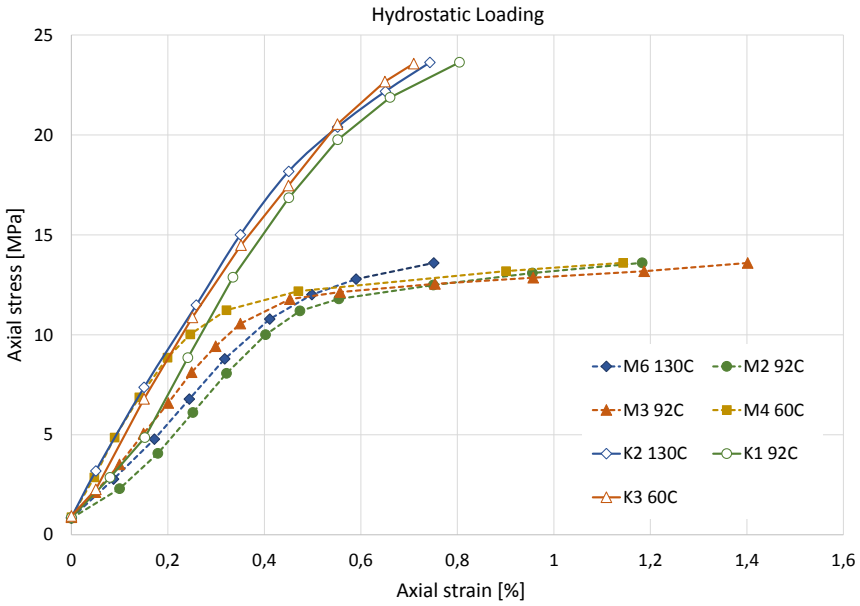

Figure 5.3: *Axial stress versus axial strain for Mons and Kansas cores. Note that the Mons cores tested at 92 and 60°C (M2, M3 and M4) had a much higher strain than the other cores.*

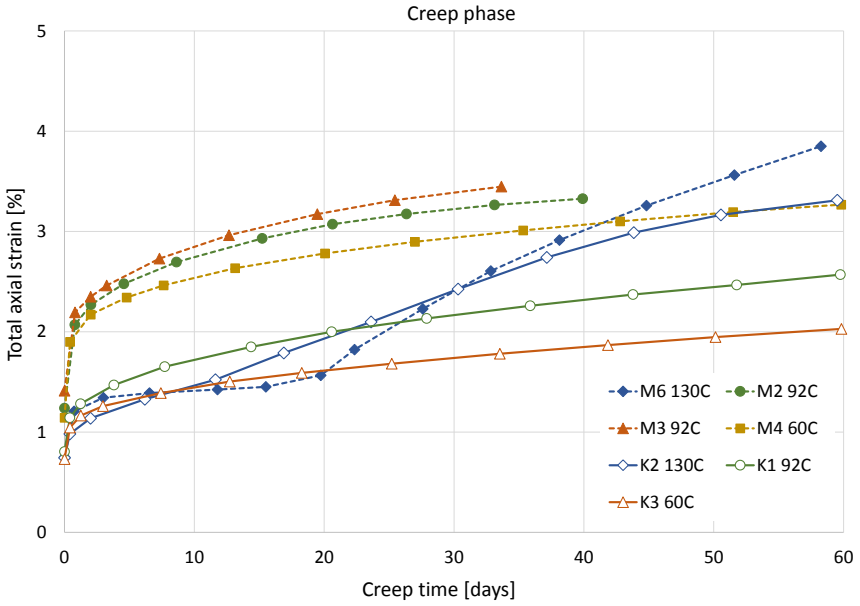

Figure 5.4: *Total axial strain versus creep time for Mons and Kansas cores.*

than the core tested at 130°C (M6) during hydrostatic loading and the first days of creep phase. As this significant temperature dependency before accelerating creep was not observed for the Kansas cores, it can be concluded that the creep behaviour of chalk is dependent both on temperature and on mineralogy.

After accelerating creep had started for the Kansas core tested at 130°C (K2) and the axial strain had exceeded the cores tested at lower temperatures (K1 and K3), strain increased with increasing temperature for Kansas cores. The difference in strain between the Kansas cores tested at 60 and 92°C (K1 and K3) became larger with time (Fig. 4.5). It can not be concluded with the same temperature dependency for the Mons cores before additional experiments are performed.

When comparing Mons and Kansas cores (Fig. 5.3 and 5.4), it can be observed that although the Mons cores are loaded to a lower confining pressure (14 MPa) than the Kansas cores (24 MPa), all Mons cores except M6 (130°C) had a much higher axial strain (1.1-1.4%) than the Kansas cores (0.7-0.8%) during hydrostatic loading. The pure Mons chalk is weaker than the impure Kansas chalk.

5.3 Chemical Aspects

By comparing ion concentration from the effluent samples for the different testing temperatures, it is obvious that the magnesium precipitation and calcium dissolution inside the cores increase with testing temperature. The effluent of the cores tested at 130°C had the lowest magnesium concentration and the highest calcium concentration, while effluent from the cores tested at 60°C had the highest magnesium concentration and lowest calcium concentration. The same temperature effect was observed for Nermoen et al. (under review) from similar experiments on outcrop chalk from the Obourg quarry in the Saint Vast formation in Belgium at 130 and 92°C. Results from SEM analysis confirmed that chemical alterations increase with increasing temperature as a higher weight percentage of magnesium was observed in the core tested at 130°C (M6) compared to the tested cores at 60°C (M4) and 92°C (K1), and K1 had a higher magnesium amount than M4 (Fig. 4.13, 4.14 and 4.15). For all the three cores the highest magnesium weight percentage was observed close to the inlet, indicating that the chemical reactions are more active there. Increased weight percentage of magnesium after flooding with $MgCl_2$ has also been observed by Zimmermann et al. (2015) and Nermoen et al. (2015), which performed tests on Liège outcrop chalk at 130°C and an effective stress of 12.6 MPa (Zimmermann et al., 2015) and 11.1 MPa (Nermoen et al., 2015). The test by Zimmermann et al. (2015) lasted for 516 days, and the inlet of the core they measured an increased MgO concentration from 0.33 to 33.03 wt%, and a corresponding depletion of CaO from 52.22 to 14.43 wt%. No significant changes in concentration of other components were observed. The

Table 5.1: *Comparison of average magnesium and calcium concentrations in the effluent from the Mons and Kansas experiment performed at 130°C in this thesis, and the experiment on Liège by Zimmermann et al. (2015).*

Chalk	Mons	Kansas	Liège
Temperature [°C]	130	130	130
Effective stress [MPa]	∼13.3	∼23.3	12.6
Testing days	60	60	516
Mg concentration [mol/l]	0.198	0.193	0.195
Ca concentration [mol/l]	0.022	0.025	0.022
Mg + Ca concentration [mol/l]	0.220	0.218	0.217
Original Mg concentration in injected brine [mol/l]	0.219	0.219	0.219

test by Nermoen et al. (2015) lasted for 1072 days, and they estimated the produced calcium amount from the core after test to be 1.12 mol out of a original amount of 1.17±0.03 mol, corresponding to 93-98% of original calcium amount. The magnesium amount retained in the core was 1.28 mol. Hence, a perfect magnesium-calcium stoichiometry was not observed, and they related the mismatch of 0.16 mol to the formation of magnesium-bearing minerals like brucite, tremolite and/or talc. In the experiments performed in this thesis, the change in magnesium and calcium concentration inside the cores was not as significant after 60 days as the observed change in Liège chalk after 516 and 1072 days by, Zimmermann et al. (2015) and Nermoen et al. (2015), respectively. In the experiment performed by Zimmermann et al. (2015) the concentration of magnesium and calcium were stable around 0.195 and 0.022 mol/l. For comparison the magnesium and calcium concentration of the tests performed on 130°C in this thesis (M6 and K1), stabilized around 0.198 and 0.022, respectively, for M6, and 0.193 and 0.025, respectively for K1 (Table. 5.1). As the concentration of magnesium and calcium in the effluent from M6, K1 and the Liège core tested by Zimmermann et al. (2015) is similar, it can be concluded that a much higher concentration change inside the cores would have been the result if the experiments in this thesis had run for a prolonged time.

In the plotted IC results (Fig. 4.7), it was observed that the curves for magnesium and calcium are mirroring each other and that the "Mg+Ca"-curve shows that the sum of magnesium and calcium concentration more or less equals the original magnesium concentration of the $MgCl_2$ brine. These observations indicate that there was a one-to-one dissolution-precipitation process between magnesium and calcium inside the cores, i.e. the stoichiometry was preserved. Results from the mass loss calculations from the IC results, agree relatively well with that. In Table 4.3 the calculated concentration of precipitated magnesium and dissolved calcium was almost equal for M6 (130°C), K1

(92°C) and M4 (60°C). Only a small amount of calcium carbonate (0.002-0.005 mol) was estimated to be dissolved during the tests.

For the experiments performed on 130°C (M6 and K2), the difference between the injected and produced concentrations was largest the first days of creep and decreases steadily for about ten days of the Mons core M6 and for about five days for the Kansas core K2. The chemical reactions inside the cores seemed to be more active in the beginning of the creep phase at 130°C. By comparing the ion concentrations and the creep curve for the M6 (Fig 5.5), it is interesting to note that there was a small decrease in magnesium concentration and a similar small increase in calcium concentration in the effluent samples at the same time as the test went into the accelerating creep phase. Clear tendency towards increase in calcium concentration in the effluent as creep started to accelerate have also been reported by others (Megawati et al., 2015; Madland et al., 2011). For K2, the same relationship between creep curve and ion concentrations is not seen that clearly (Fig. 5.6). Magnesium and calcium concentration in effluent is more of less constant when the creep accelerates, but it should be noted that K2 also had a less pronounced creep acceleration.

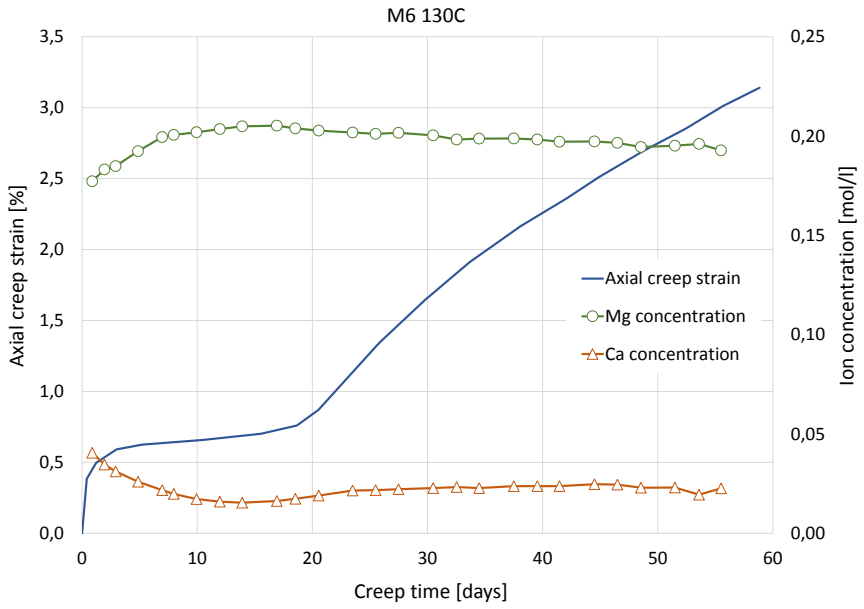

Figure 5.5: *Axial creep strain plotted together with magnesium and calcium concentration measured in effluent water from M6 tested at 130°C. Note the small decrease in magnesium concentration and a similar small increase in calcium concentration as creep accelerates.*

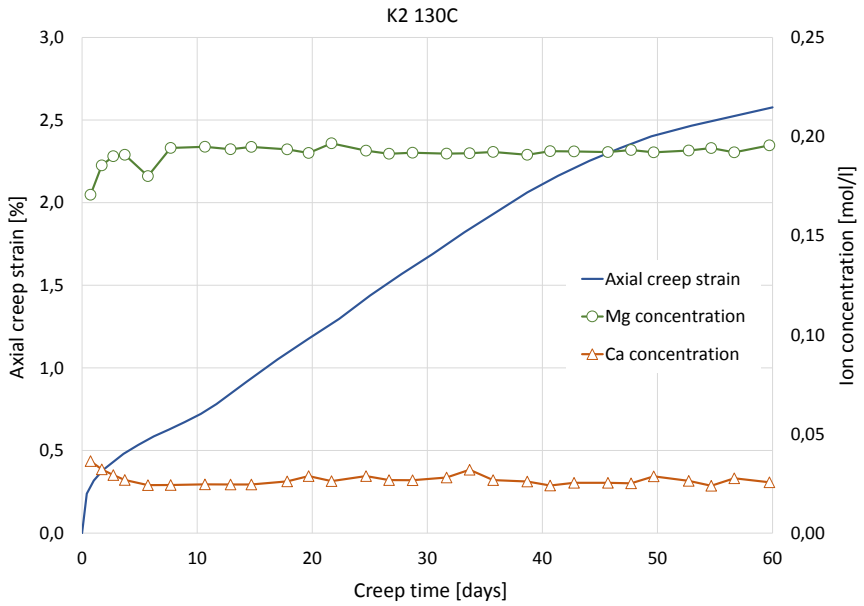

Figure 5.6: *Axial creep strain plotted together with magnesium and calcium concentration measured in effluent water from K2 tested at 130°C. Ion concentrations was more or less stable when creep started accelerating.*

5.4 Effect of Cleaning the Cores with Distilled Water After $MgCl_2$ Flooding

A clear behavioural difference between the first three experiments (M6 130°C, K1 92°C and M4 60°C) was observed when the mechanical tests were finish and the flooding was switched from $MgCl_2$ to distilled water (DW) in order to clean the cores. The other experiments either failed (M2) or are still running (M3, K2 and K3), and are therefore not included in this discussion. In Fig. 5.7 axial creep strain is plotted against creep time for the first three experiments. The circles indicate the time when flooding was switched from $MgCl_2$ to DW, and dashed lines indicate the trend-line of the creep strain if $MgCl_2$ flooding had continued. Only minutes after DW flooding started in M6 (130°C), the deformation stopped and became constant, while for the cores K1 (92°C) and M4 (60°C) deformation continued after DW flooding had started, the deformation rate even increased slightly for both cores. As the two Mons cores (M6 and M4) behaves differently, this effect is most probably not an effect of chalk type. The results rather indicate that this effect is temperature dependent. Nermoen et al. (2015) also observed a reduction in deformation when injection brine was switched from $MgCl_2$ to DW in a Liège core tested at 130°C. The Liège core did not stop deforming, but the deformation rate was significantly reduced.

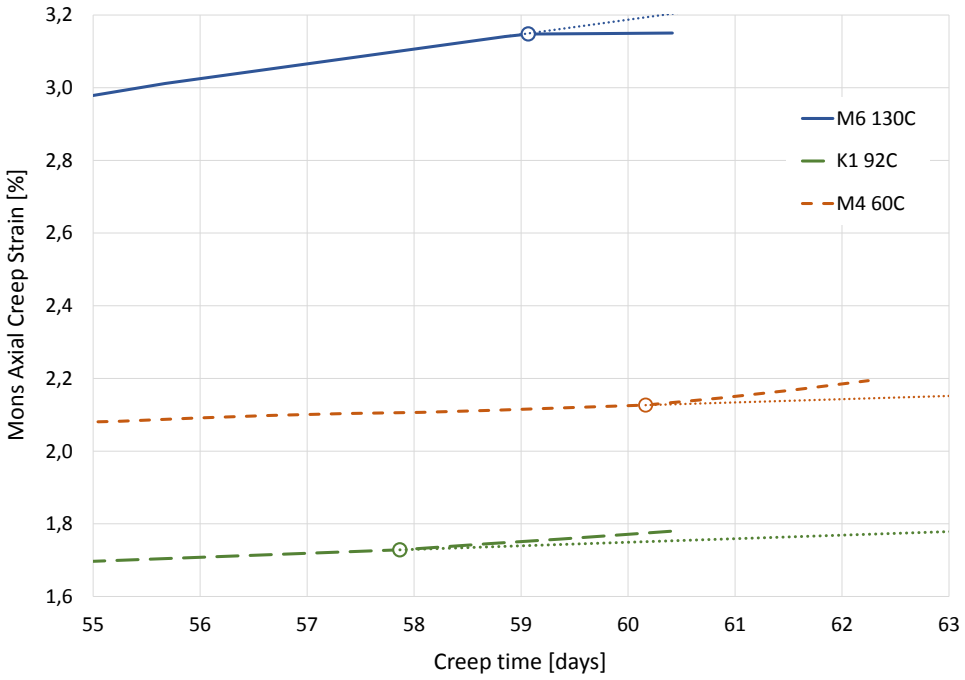

Figure 5.7: *Axial creep strain versus creep time for Mons cores M6 (130°C) and M4 (60°C) and Kansas core K1 (92°C). The circles on each graph illustrates the time when flooding was switched from $MgCl_2$ to DW. Note that deformation of M6 stops when DW is injected, while the deformation of M4 and K1 continued to increase.*

5.5 Effect of Temperature on Core Measurements Before and After Testing

The precipitation-dissolution process between magnesium and calcium cause a lowering in core mass loss because magnesium has a lower molar weight than calcium. In the previous discussed results it was seen that the dissolution-precipitation process increased with increasing temperature. Mass loss calculations from both IC data and from weight difference of dry core before and after testing had a corresponding temperature dependency as M6 (130°C) had a higher mass loss than K1 (92°C), which again had a higher mass loss than M4 (60°C). The change in mass was also seen to affect the change in bulk volume, density and porosity. As Mons and Kansas have differences in chalk properties and because Mons and Kansas cores were tested at different stresses (14 and 24 MPa, respectively), it is more correct to exclude K1 for the following comparison. M6 (130°C) had a larger decrease in bulk volume and a large increase in density compared to M4 (60°C)(Table 4.7 and 4.9). For M4 no significant difference was observed in average density for unflooded chalk and the tested core from the gas pycnometer measurements (Eq. (2.15) and (2.16)). Although no change in density was observed, the core mass was reduced after testing. This mass reduction can be explained by erosion of chalk due to non-equilibrium reactions between the injected brine and the

chalk. Fig. 5.8 show erosion at the inlet side of M6 (130°C) where the injected brine had flooded out of the holes in the drainage plate. Similar eroded holes was also observed for M4 (60°C) and K1 (92°C). For M6 the density of unflooded chalk was not estimated by the method of gas pycnometer measurements, but the original density (2.69 g/cm^3) was estimated before testing from the weight difference in dry and saturated weight (Eq. (2.14)). When estimating density of M6 after testing by the method of gas pycnometer measurements, the average density from all methods (2.70-2.72 g/cm^3) was higher than original density. Due to the uncertainty of correct measurement of the chalk volume of the small chalk pieces in the gas pycnometer, it is impossible to conclude if a higher density was measured by the inlet side of M6 or not.

Figure 5.8: *Erosion of M6 at the inlet side where the brine have been flooded out of the holes in the drainage plate. Similar erosions was also observed for M4 and K1.*

Porosity calculation from method 1 (Eq.(2.11)) where porosity was estimated based on weight difference between dry and saturated core and the solid density after testing, gave almost the same porosity reduction for M6 (130°C) and M4 (60°C)(Table 5.2). Porosity estimation by Method 2 (Eq.(2.12)), where porosity calculations were based on change in volumetric strain, gave a higher porosity reduction for M6 (130°C) of 4.0% compared to a reduction of 3.3% for M4 (60°C). Hence, a temperature affect on porosity can be observed in this thesis dependent on the method used in the calculation. Also for K1 (92°C), there was a significant different in the calculated porosity between method 1 and 2. Wang et al. (under review) performed experiments where two Liège cores were flooded with $MgCl_2$ and NaCl at 130°C. For the core flooded with $MgCl_2$ Wang et al. (under review) also observed that the porosity calculation from method 2 (from volumetric changes) gave a significantly higher porosity reduction compared to method 1 (from mass difference between dry and saturated core and new density estimation). The same significant difference in porosity after testing was not observed for the core flooded with NaCl. The small porosity difference after flooding with NaCl was explained by more or less only compaction and no chemical alteration (Wang et al., under review). $MgCl_2$ is a reactive fluid in contact with chalk, while NaCl is close to non-reactive. Hence, when flooding with $MgCl_2$, the porosity development is complex since neither the solid volume nor the bulk volume are conserved. Both compaction and chemical alterations of the core need to be accounted for in the porosity calculations. Method 2 where porosity calculations was only based on volumetric changes is therefore inadequate for porosity calculations in this thesis where chemical

reactions occurred.

Table 5.2: *Comparison of porosity before and after testing of Mons cores M6 (130° C) and M4 (60° C) and Kansas core K1 (92° C).*

Core		M6	K1	M4
Original porosity [%]	Method 1	42.2	36.5	42.5
New porosity [%]	Method 1	39.6	34.0	39.7
	Method 2	38.2	33.3	39.2
Porosity change [%]	Method 1	2.6	2.5	2.8
	Method 2	4.0	3.2	3.3

5.6 pH Analysis

From the plot of pH versus creep time presented in the results(Fig. 4.9), it was difficult to see any trends or temperature dependencies between the experiments as the pH was fluctuating a lot, and a suspicion against the pH meter was mentioned in the results. This suspicion have been further investigated by plotting pH against the sampling date to see if that would provide new information (Fig. 5.9). The new plots clearly show that the pH that is measured at the same dates are fluctuating together, indicating that the fluctuation is manly due to the pH meter and not actual fluctuation of the pH of the effluent. As the pH meter gave such fluctuating values, it is impossible to know the exact pH for each date. For future experiments, the pH meter should be calibrated daily before the measurements in order to reduce the risk of wrong pH measurements. In this thesis, the pH meter was calibrated approximately once a week. There was not observed fluctuation in pH for the effluent samples that was used for IC analysis (Fig. 4.10). The reason is probably that after the IC analysis, these effluent samples were stored for several weeks before the pH of all of them was measured at the same day, i.e. no pH meter error caused fluctuations.

Regarding temperature trends, it can be observed in Fig. 5.9a that M6 (130°C) for all dates had a lower pH than M4 (60°C), and in Fig. 5.9b that K2 (130°C) for all dates had a lower pH than K3 (60°C). These results indicate that pH of the effluent is lower for tests performed at 130°C than 60°C. The cores tested at 92°C (K1, M2 and M3) was not included in the comparison above since there was no other Kansas cores tested at the same time as K1 and no other Mons cores tested at the same times as M2 and M3. Although the exact pH values of the effluent cannot be determine from the data due to uncertainty of the pH meter, it is observed that the pH of the effluent from the tests at 130°C (M6 and K2) generally was right below 6 and the pH of effluent from the tests at 60 and 92°C (M2, M3, M4, K1 and K3) generally was right above 6 (6.1-6.5). The pH of injected

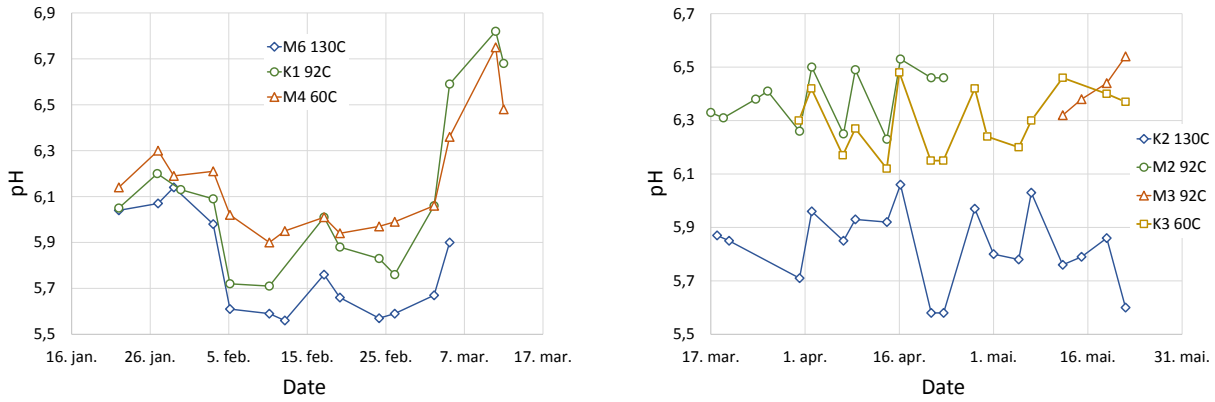

(a) (b)

Figure 5.9: *Measured pH of effluent samples plotted against the date of sampling. The three first experiments (M6, K1 and M4) in plot a) and the failed M2 and the experiments that are still running (K2, M3 and K3) in plot b). Note that pH is fluctuating together.*

brine was between 5.5 and 6.0. Hence, the pH of the effluent from the tests at 130°C was not affected by the chemical alterations inside the core, while the effluent of the experiments at 60 and 92°C increased slightly compared to injected brine pH. One possible explanation if that minerals like brucite precipitate at high temperature (130°C), which causes the pH of the effluent to decrease compared to the effluent from cores tested at lower temperatures.

The pH of the effluent samples that was measured almost daily over time showed that the pH increases from about 6 to 8 in 2-3 weeks. There have not been time to study the exact reason for this pH increase, but result from a quick simulation in PHREEQC Pitzer indicated that the effluent not is in equilibrium when it comes out of the core, which causes dissolution of new mineral phases that causes changes in pH over time. Further pH analysis should be performed to determine which chemical reactions that occur in the effluent. In addition it would have been interesting to analyse how sensitive the effluent pH is to the air gap inside the sampling glasses. Effluent samples of different volumes can be collected and analysed over time to see if there are an observed difference in pH evolution, or they can be sealed tightly after collection and stored for some time (days of weeks) before measurement to see if effluent pH will increase equally much for each samples or not.

5.7 Permeability Evolution

Permeability was observed to decrease with increasing strain (Fig. 4.4 and 4.6). The higher the deformation rate, the higher the reduction rate of permeability. When core M6 (130°C) had a steady state creep, the permeability seemed to stabilize. These observations indicated a dependency between compaction and permeability. Observations by Nermoen et al. (2015), on the other hand, showed that permeability not only is dependent on compaction, but also the dissolution processes inside the core. During a 1072 day long $MgCl_2$ flooding experience with Liège chalk at 130°C, the flooding rate was changed between 33.12 and 99.36 ml/min (one and three PV's per day, respectively) four times throughout the test. The test started with a flooding rate of 33.12 ml/min, and the permeability decreased as the core compacted. When the flooding rate was changed to 99.36 ml/min, the compaction continued, but now the permeability increased. Nermoen et al. (2015) explained the observed increase in permeability to be caused by a shift from volumetric dominated compaction to dissolution dominated compaction as the flooding rate increased. Compaction alone causes pore volume in chalk to reduce resulting in reduced permeability, while dissolution processes alone causing the pore volume to increase resulting in increased permeability. Hence, if the compaction overcome the effect of dissolution, pore volume and permeability are expected to reduce, and vice versa.

The permeability calculations showed unexpected fluctuations. For core M3 (92°C), M4 (60°C), K1 (92°C) and K3 (60°C) there was observed a jump in the permeability at the exact same time as the brine in the flooding cells was refilled. Although the brine inside the flooding cell was pressurized to pore pressure before connecting it to the flooding system, the differential pressure dropped causing a jump in permeability. After the brine change, it took the differential pressure a long time (several days to weeks) to build up to its previous value. For the first brine refill of K1 (Fig. 4.6b at 20 creep days) the differential pressure never reached its previous value before the next brine refill made the differential pressure decrease again. A suggestion to avoid such problems in future experiments is to connect an additional pressure gauge to the flooding cell to measure the pressure at the outlet of the cell. In the experiments performed in this thesis, the pressure in the flooding cell was controlled by the pump settings. By using a more accurate pressure gauge to control the pressurization process of the flooding cell after brine refill, the drop in differential pressure over the core can may be avoided when the flooding cell is reconnected to the flooding system into the core.

The permeability of K2 (130°C) is plotted together with differential pressure and creep strain against creep time in Fig. 5.10. The permeability dropped to almost zero after 22 creep days due to an unexpected increase in the differential pressure. The differential pressure increased slowly in the beginning of the creep phase, but after 22 days it started increasing much faster and after some

time it stabilized at about 0.15 MPa. As the experiment is still running, the exact reason for the increased differential pressure is not known, but there are most likely something clogging in the flow patterns in the core. In Fig. 5.10 it can be observed that after some time with high differential pressure, the deformation rate starts to decrease. Before the differential pressure increased, the core experienced an effective pressure of 23.3 MPa (confining pressure - pore pressure = 24 MPa - 0.7 MPa, when assuming that the Biot coefficient is equal to one). By assuming that the clogging was located at the outlet of the core, the core experienced a lower effective stress of 23.15 MPa (24 - 0.7 - 0.15) with the increased differential pressure. Although the difference in effective stress is relatively small, the core seemed to compact less.

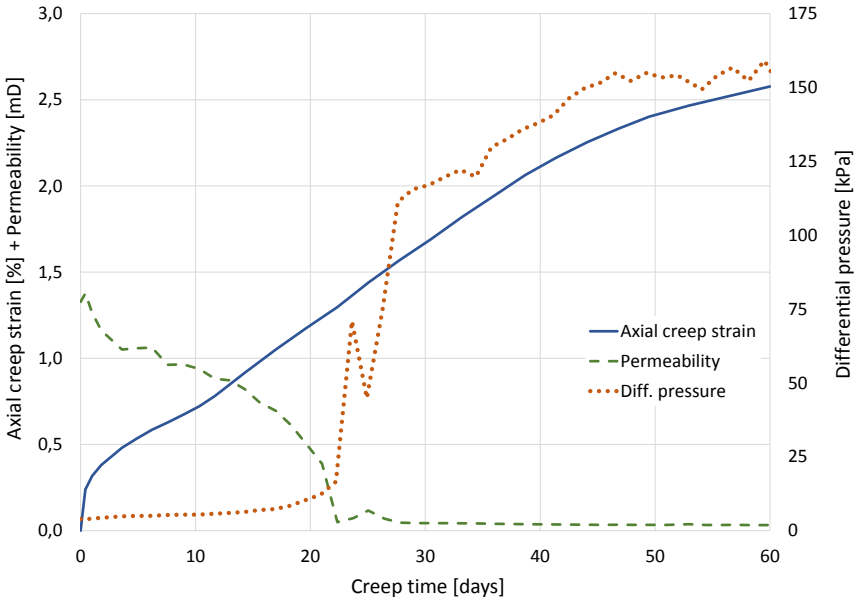

Figure 5.10: *Axial creep strain plotted together with permeability and differential pressure for K2 tested at 130°C. At 22 creep days the differential pressure had an abrupt increase causing the permeability to drop to almost zero.*

The permeability for M3 (92°C) had a big drop during the first creep day (Fig. 4.4c). The reason for the drop seem to be related to the permeability evolution of M3 during hydrostatic loading. In Fig. 5.11 axial stress is plotted against permeability for all Mons cores. While the other Mons cores (M2, M4 and M6) had a permeability of 1.07-1.16 mD at the end of the hydrostatic loading, M3 had a permeability of 1.90 mD. M3 had the same trend in permeability reduction as the other cores in the beginning of the hydrostatic loading, but after loading to 12 MPa something caused the permeability to increase to over 2.50 mD. After this incident, the permeability decreased again at a high rate, but as the permeability did not reach the same value as the other Mons cores it seemed to continue the abrupt decrease into the creep phase (Fig. 4.4c). The incident causing the

permeability to make a jump during hydrostatic loading was that the flooding pump head and valve was cleaned and in addition the bypass was kept open for some minutes. The reason was that the pump did not deliver the correct flooding rate, and that problem was attempted solved. After the first creep day the abrupt permeability decrease stopped and a slow permeability reduction was seen throughout the test.

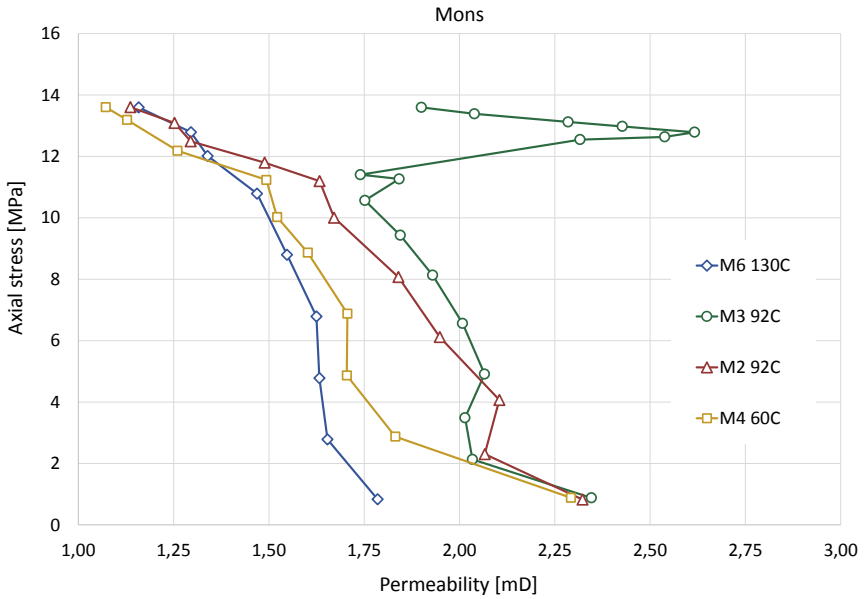

Figure 5.11: *Stress versus permeability during hydrostatic loading for Mons cores.*

6 Concluding Remarks and Future Work

6.1 Conclusion

The objective of this thesis was to study the effect of different temperature and chalk types. This was done by performing mechanical tests on Mons (Belgium) and Kansas (Niobrara, US) outcrop chalk during injection of 0.219 M $MgCl_2$ brine at 60, 92 and 130°C. The tests were performed by loading the cores hydrostatically above yield followed by a 60 day creep phase with a confining pressure of 14 MPa for Mons cores and 24 MPa for Kansas cores. Pore pressure was 0.7 MPa for both Mons and Kansas cores. Fractioned effluent was chemically analysed and three of the tested cores were studied by SEM-EDS.

From the reported results, the following conclusions can be drawn:

- Chalk behaviour during mechanical tests is dependent both on chalk type as well as temperature. During hydrostatic loading Kansas chalk behaved similar for all temperatures, while the Mons core tested at 130°C actually had a lower compaction than the Mons cores tested at lower temperatures; 60 and 92°C. At 130°C Mons chalk had a significant delayed compaction response, but as accelerating creep started the compaction had an abrupt increase and exceeded the compaction of the Mons cores tested at 60 and 92°C. Accelerating creep was only observed for tests performed at 130°C for both Mons ans Kansas chalk. During creep phase compaction of Kansas cores increased with increasing temperature, while it could not be concluded with the same temperature dependency for the Mons cores at 60 and 92°C before more additional experiments are performed.

- Magnesium and calcium was seen to have a one-to-one dissolution-precipitation process inside the cores. Chemical alteration increased with increasing temperature for both Mons and Kansas, and the chemical alteration was observed to be highest by the inlet of the cores, which confirms the previous studies at the University of Stavanger (Zimmermann et al., 2015; Nermoen et al., 2015). In the Mons core tested at 130°C, growth of magnesite minerals were found.

- Core mass loss during testing was observed to increase with increasing temperature. As precipitation of magnesium replace dissolved calcium, the chalk loose mass since magnesium has a lower molecular weight than calcium. Also bulk modulus decreases with increasing temperature, while density increases. Porosity and permeability evolution is dependent on both compaction of the chalk and the dissolution process inside the chalk. When compaction overcomes dissolution, porosity and permeability is seen to decrease.

- Accelerating creep is connected to chemical activity. For Mons chalk tested at 130°C, the difference between magnesium and calcium concentration in effluent compared to the injected $MgCl_2$ brine decreased when accelerating creep started.

- The pH of effluent from chalk flooded with $MgCl_2$ at 130°C is unaffected by the chemical alterations inside the chalk, while the pH of the effluent from chalk tested at lower temperatures (60 and 92°C) increase slightly compared to the injected brine pH.

6.2 Future Work

- More experiments should be performed on Mons chalk to confirm the observed trend towards lower bulk modulus with increasing temperature and to determine if there is a difference in creep strain for tests performed at 60 and 92°C.

- The mechanisms of the observed accelerating creep at 130°C is not understood. More experiments should be run on different chalk types at different temperatures. Especially temperatures between 92 and 130°C is of interest, to determine a more exact temperature of when accelerating creep is observed for different chalk types. Both pure and impure chalk should be tested to see if there is a connection between mineralogy and accelerating creep.

- Chemical analysis of effluent from flooding experiments with $MgCl_2$ should performed to determine the reason for why the pH of effluent from tests performed at 130°C is lower than the effluent from tests performed at 60 and 92°C.

References

CREWES (2015), University of Calgary. Available from: http://www.crewes.org/ResearchLinks/ExplorerPrograms/FlProp/FluidProp.htm [23.05.2015].

Dandekar, A. Y. (2006), *Petroleum Reservoir Rock and Fluid Properties*, Taylor & Francis Group.

Davidsen, A. (2011), A Mechanical Study of the effect of Sulphate, Master's thesis, The Faculty of Science and Technology, University of Stavanger.

Delage, P., Cui, Y. J. and Schroeder, C. (1996), 'Subsidence and Capillary Effects in Chalk', *ISRM Conference Paper* .

Fjær, E., Holt, R. M., Horsrud, P., Raaen, A. M. and Risnes, R. (2008), *Petroleum Related Rock Mechanics*, 2nd edn, Elsevier, Oxford, UK.

Heggheim, T., Madland, M. V., Risnes, R. and Austad, T. (2004), 'A Chemical Induced Enhanced Weakening of Chalk by Seawater', *Journal of Petroleum Science and Engineering* **Vol.46**, pp.171–184.

Hellmann, R., Renders, P. J. N., Gratier, J.-P. and Guiguet, R. (2002), 'Experimental Pressure Solution Compaction of Chalk in Aqueous Solutions - Part 1. Deformation Behaviour and Chemistry', *The Geochemical Society, Special Publication* (No. 7), pp.129–152.

How SEM-EDS Works (n.d.), SEAL Laboratories, Evans Analytical Group. Available from: http://www.seallabs.com/how-sem-eds-works.html [23.05.2015].

Kennedy, W. J. (1985), Sedimentology of the Late Cretaceous and Early Palaeocene Chalk Group, North Sea Central Graben, *in* 'North Sea Chalk Symposium May 1985: 1'.

Kjørslevik, T. A. C. and Østensen, G. (2014), 'The Effect of Stress Level and Temperature on Water Weakening of Chalk'. Bachelors Thesis.

Korsnes, R. I., Madland, M. V. and Austad, T. (2006a), Impact of Brine Composition on the Mechanical Strength of Chalk at High Temperature, *in* 'Eurock 6: Multiphysics Coupling and Long Term Behaviour in Rock Mechanics', Taylor & Francis, pp. 133–140.

Korsnes, R. I., Madland, M. V., Austad, T., Haver, S. and Røsland, G. (2007), 'The Effects of Temperature on the Water Weakening of Chalk by Seawater', *Journal of Petroleum Science and Engineering* **Vol.60**, pp.183–193.

Korsnes, R. I., Wersland, E., Austad, T. and Madland, M. V. (2006b), 'Anisotropy in Chalk Studied by Rock Mechanics', *Journal of Petroleum Science and Engineering* .

Madland, M. V., Hiorth, A., Omdal, E., Megawati, M., Hildebrand-Habel, T., Korsnes, R. I., Evje, S. and Cathles, L. M. (2011), 'Chemical Alterations Induced by Rock-Fluid Interactions When Injecting Brines in High Porosity Chalks', *Transport in Porous Media* **Vol.87**(3), pp.679–702.

Mathiesen, E. (2005), 'Ekofisk: Levende museum', Oljedirektoratet. Available from: http://www.npd.no/no/nyheter/nyheter/2005/ekofisk-levende-museum--/ [12.05.2015].

Megawati, M., Hiorth, A. and Madland, M. V. (2012), 'The Impact of Surface Charge on the Mechanical Behaviour of High-Porosity Chalk', *Rock Mechanics and Rock Engineering* **Vol.46**, pp.1073–1090. DOI 10.1007/s00603-012-0317-z.

Megawati, M., Madland, M. V. and Hiorth, A. (2015), 'Mechanical and Physical Behaviour of High-Porosity Chalks Exposed to Chemical Perturbation', *Journal of Petroleum Science and Engineering* .

Nermoen, A., Korsnes, R. I., Aursjø, O., Madland, M. V., Kjørslevik, T. A. C. and Østensen, G. (under review), 'How Stress and Temperature Conditions Affect Rock-fluid Chemistry and Mechanical Deformation', *Frontiers in Physics, Interdisiplinary Physics* .

Nermoen, A., Korsnes, R. I., Christensen, H. F., Trads, N., Hiort, A. and Madland, M. V. (2013), 'Measuring the Biot Stress Coefficient and Its Implications on the Effective Stress Estimate', *ARMA 13-282, American Rock Mechanics Assosiation* pp. pp.1–9.

Nermoen, A., Korsnes, R. I., Hiorth, A. and Madand, M. V. (2015), 'Porosity and Permeability Development in Compacting Chalks During Flooding of Nonequilibrium Brines: Insight from Long-term Experiment', *Journal of Geophysical Research: Solid Earth* . DOI 10.1002/2014JB011631.

Newman, G. H. (1985), 'The Effect of Water Chemistry on the Laboratory Compression and Permeability Characteristics of Some North Sea Chalks', *Journal of Petroleum Technology, SPE-10203-PA* **Vol.35**.

Risnes, R. and Flaageng, O. (1999), 'Mechanical Properties of Chalk with Emphasis on Chalk-Fluid Interactions and Micromechanical Aspects', *Oil and Gas Science and Technology* **Vol.54**(6), pp.751–758.

Risnes, R., Haghighi, H., Korsnes, R. I. and Natvik, O. (2003), 'Chalk-fluid Interactions with Glycol and Brines', *Tectonophysics* **Vol.370**, pp.213–226.

Risnes, R., Madland, M. V., Hole, M. and Kwabiah, N. K. (2005), 'Water Weakening of Chalk - Mechanical Effects of Water-glycol Mixtures', *Journal of Petroleum Science and Engineering* **Vol.48**, pp.21–36.

Tobiesen, E. (2013), 'Flooding MgCl2 into High Porosity Outcrop Chalk'. Bachelors Thesis.

Wang, W., Madland, M. V., Zimmermann, U., Bertolino, S. R. A., Hildebrand-Habel, T., Korsnes, R. I. and Nermoen, A. (under review), Revealing Dynamic Porosity: Evaluation of Porosity During Chemo-mechanical Compaction in Chalk from Liège (Belgium).

Zimmermann, U., Madland, M. V., Nermoen, A., Hildebrand-Habel, T., Bertolino, S. R. A., Hiorth, A., , Korsnes, R. I., Audinot, J.-N. and Grysan, P. (2015), 'Evaluation of the Compositional Changes During Flooding of Reactive Fluids Using Scanning Electron Microscopy, Nano-secondary Ion Mass Spectromatry, X-ray Diffraction, and Whole-rock Geochemistry', *The American Association of Petroleum Geologists* **Vol.99**(No.5), pp.791–805.

Zornes, D. R. (2004), 'A Perspective on Experience on U.S-Norwegian Co-operation on EOR at COREC Centre at Rogaland and University of Bergen', PowerPoint presentation, ConocoPhillips.